Salmonella SopB suppresses post-transcriptionally regulated cytokine release to reduce early tissue inflammation and delay disease progression

Nour Diab[1], Chiun Huei Yong[1], Eva-Lena Stange[1], Marlène Birk[1], Matthias Schmitz[1], Stefan Düsterhöft[2§], Jonas Pes[1], Kira Noemi Ferle[1], Isabel Karkossa[3], Kristin Schubert[3], Jörg Deiwick[4], Mihael Vucur[5], Tom Luedde[5], Natalia Torow[1,6], Andreas Ludwig[2], Aline Dupont[1], Joel Selkrig[1], Martin von Bergen[3], Michael Hensel[4], Kaiyi Zhang[1*], Mathias W. Hornef[1,7*]

[1] Institute of Medical Microbiology, RWTH Aachen University Hospital, 52074 Aachen, Germany
[2] Institute of Molecular Pharmacology, RWTH Aachen University Hospital, 52074 Aachen, Germany
[3] Department Molecular Toxicology, Helmholtz Centre for Environmental Research GmbH - UFZ, Leipzig, Germany
[4] Division of Microbiology, University of Osnabrück, Osnabrück, Germany
[5] Department of Gastroenterology, Hepatology, and Infectious Diseases, Medical Faculty, Heinrich-Heine-University, Düsseldorf, Germany
[6] Helmholtz Centre for Infection Research, Inhoffenstr. 7, 38124 Braunschweig
[7] Euregional Microbiome Center, RWTH Aachen University Hospital, 52074 Aachen, Germany

[§]Present address: HMU Health and Medical University Düsseldorf-Krefeld, Düsseldorf, Germany

Short title: The anti-inflammatory effect of *Salmonella* SopB

Word count: 9303 words including main text, references, and figure legends but excluding material and methods.

Abbreviations: *Salmonella* Typhimurium, *S.* Typhimurium; *Salmonella* outer protein B, SopB; tumour necrosis factor alpha, TNFα; a disintegrin and metalloprotease 17 (ADAM17); mechanistic target of rapamycin, mTOR.

Access to datasets: The mass spectrometry proteomics data have been deposited to the ProteomeXchange Consortium via the PRIDE partner repository with the dataset identifier PXD045931 and 10.6019/PXD045931. Transcriptomic data have been deposited at GEO with the accession number GSE300992 (GSM9073322-GSM9073332) and GSE326693.

Conflict of interest statement: All authors agree to the submission. The submitted material has not been previously reported and is not under consideration for publication elsewhere. There are no competing financial interests for any of the authors of this manuscript.

Funding sources: Priority Program SPP2225 (project ID P446460159, to M.W.H. and project ID 446414114 to M.H.), a research grant (project ID 279874820, LU1360/3-2 to T.L.), the Collaborative Research Centers CRC1382 (project ID 403224013-SFB 1382 to M.W.H., M.v.B.), CRC/TRR 359 (project ID 491676693-SFB/TRR359 to M.W.H.) and CRC1557 (project ID 467522186, SFB1557 to M.H.) from the German Research Foundation (DFG), the project 'Microbial Stargazing – Erforschung von Resilienzmechanismen von Mikroben und Menschen' (project ID 01KX2324, to N.T.) from the Federal Ministry of Research, Technology and Space (to N.T.), a research grant (project ID 70114893 to M.V.) from the German Cancer Aid and the ERC Advanced Grant EarlyLife (project ID: 101019157 to M.W.H.) from the European Research Council, support by the START-Program of the Faculty of Medicine at RWTH Aachen University.

* Corresponding authors: Mathias W. Hornef, M.D. and Kaiyi Zhang, Ph.D., Institute of Medical Microbiology; RWTH Aachen University Hospital; Pauwelsstr. 30, D-52074 Aachen, Germany. Phone: *49 241 80 89510; Fax: *49 241 80 82483; E-mail: mhornef@ukaachen.de and kzhang@ukaachen.de
ORCID ID: 0000-0001-6096-9110 and 0000-0002-0525-5817.

Abstract

Salmonella enterica subsp. *enterica* serovar Typhimurium (*S.* Typhimurium) manipulates cellular processes through the translocation of effector molecules into the host cell cytosol. Using a recently established neonatal *S.* Typhimurium infection model, we provide functional insights into how *Salmonella* outer protein B (SopB) suppresses early mucosal tissue inflammation and prolongs host survival. Mechanistically, SopB prevents a disintegrin and metalloprotease 17 (ADAM17) activation, plasma membrane translocation and the release of membrane-bound TNFα from enterocytes and reduces epithelial secretion of IL-18 *via* mTOR-controlled secretory autophagy. This abolishes the early epithelial transcriptional response and reduces immune cell recruitment and programmed cell death-mediated mucosal barrier disruption delaying disease progression. The immunosuppressive effect of SopB is independent of the C-terminally encoded phosphatidylinositol phosphatase and phosphotransferase activity but requires an intact N-terminal domain. Thus, here we demonstrate that SopB suppresses the early, post-transcriptional regulation of epithelial cytokine release in an inositol phosphatase-independent manner likely promoting pathogen transmission.

(150 words)

Keywords: neonate; *Salmonella* Typhimurium; intestinal epithelium; *Salmonella* outer protein (Sop)B; programmed cell death; tumour necrosis factor alpha (TNFα); a disintegrin and metalloprotease 17 (ADAM17)/tumour necrosis factor-alpha converting enzyme (TACE); secretory autophagy; mechanistic target of rapamycin (mTOR)

Introduction

Salmonella enterica subsp. *enterica* sv. Typhimurium (*S.* Typhimurium) is an important human enteropathogen with a high disease burden in children and neonates worldwide (Das et al., 2021). It uses the *Salmonella* pathogenicity island (SPI)1-encoded type three secretion system (T3SS) to translocate effector molecules into intestinal epithelial cells. These effector molecules induce bacterial internalisation, shape formation of the *Salmonella*-containing vacuole (SCV) and manipulate host cell processes to promote intracellular survival and proliferation (LaRock et al., 2015; Zhang et al., 2014; Zhang et al., 2018). Among the effector molecules translocated by the SPI1-T3SS is SopB, a phosphatidylinositol phosphate 4 and 5 (PtdIns(4,5)P_2) phosphatase and phospho-transferase/isomerase that generates PtdIns(3,4,5)P_3 and PtdIns(3,4)P_2 in a non-canonical phosphoinositide 3-kinase (PI3K)-independent manner (Norris et al., 1998; Terebiznik et al., 2002; Walpole et al., 2022).

Through its C-terminal phosphatase domain (aa 357-561), SopB together with SopE/SopE$_2$ activates the Rho GTPases Cdc42 (Zhou et al., 2001), enriches RhoJ, RhoB, RhoH and R-Ras1 (Truong et al., 2018), PtdIns(3,4)P_2 and PtdIns(3,4,5)P_3 (Mallo et al., 2008), Arf GEF ARNO (Humphreys et al., 2012), annexin A2 (Jolly et al., 2014; Rescher et al., 2004), Myo6 (Brooks et al., 2017), as well as SNX9 (Piscatelli et al., 2016) and SNX18 (Liebl et al., 2017) at the entry site, leading to actin remodelling, ruffling, membrane fission and uptake by intestinal epithelial cells, the first step in invasive infection (Hanisch et al., 2011; Terebiznik et al., 2002). SopB is then multi-mono-ubiquitinated and recruited to the endosomal membrane, where it reduces the negative surface charge of the *Salmonella*-containing vacuole (SCV) by removing PtdIns(4,5)P_2 and phophatidylserine, thereby inhibiting Rab recruitment and lysosomal fusion (Bakowski et al., 2010; Drecktrah et al., 2005; Hernandez et al., 2004; Patel et al., 2009). Additionally, SopB induces a sustained phosphatase-dependent Akt phosphorylation protecting infected cells from cell death (Drecktrah et al., 2005; Finn et al., 2017; Knodler et al., 2005;

Marcus et al., 2001; Roppenser et al., 2013; Ruan et al., 2016; Steele-Mortimer et al., 2000). SopB expression persists for many hours *in vivo* (Drecktrah et al., 2005; Giacomodonato et al., 2011). More recently, the N-terminal GTPase binding domain (residues 117-168) of SopB has been shown to facilitate phosphatase-independent interaction with Cdc42 leading to actin fibre disruption, cell cycle arrest and MAP kinase signalling in yeast cells (Aleman et al., 2005; Burkinshaw et al., 2012; Rodriguez-Escudero et al., 2011; Rodriguez-Escudero et al., 2006; Rogers et al., 2008). However, the functional role of SopB during *in vivo* infection and in particular the influence of the N-terminal domain has not been investigated.

Using our oral neonatal mouse infection model that requires SPI1-dependent enterocyte invasion (Zhang et al., 2014), we have previously shown that SopB is not required for enterocyte invasion and SCV formation (Zhang et al., 2018). Here, we analysed the role of SopB during the early course of the disease using isogenic mutant strains, co-culture experiments with polarised m-IC_{cl2} cells and intestinal epithelial stem cell organoids, and oral infection of mice deficient in innate immune signalling and cell death pathways in combination with flow cytometry, global phosphoproteome and transcriptome analyses, affinity enrichment of SopB-associated host proteins by mass spectrometry as well as AlphaFold-Multimer (AFM) protein-protein interaction prediction. Unexpectedly, we observed an accelerated disease progression and increased mortality after infection with SopB-deficient *S.* Typhimurium. A detailed analysis revealed a suppressive effect of SopB on a disintegrin and metalloprotease 17 (ADAM17)/TNF converting enzyme (TACE) activity and secretory autophagy reducing early cytokine release with subsequent reduction of chemokine expression and immune cell recruitment, decreased enterocyte cell death and prolonged host survival.

Material and Methods

Bacterial strains

In this study, wild-type (wt) *Salmonella enterica* subsp. *enterica* serovar Typhimurium (ATCC14028, *S.* Typhimurium), an isogenic Δ*sopB* mutant strain, Δ*sopB* mutant strains complemented with *sopB* (Δ*sopB,* p*sopB*) or *sopB* and its chaperon *sigE* (Δ*sopB,* p*sopBsigE*), an isogenic Δ*sopE*$_2$ mutant strain (Zhang et al., 2018), as well as strains carrying chromosomal alleles with point mutations encoding SopB with exchanges in the C-terminal domain at position 460 (C460S, SopB^{C460S}) or 528 (K528A, SopB^{K528A}) or in the N-terminal domain in position 76 (L76P, SopB^{L76P}) were used (Suppl. Table 1). Low copy number plasmid p4042 has been introduced before (Zhang et al., 2018) and was shown to restore function of deleted sopB. pP4042 was used as template for site-directed mutagenesis using Q5 site-directed mutagenesis kit (NEB) according to manufacturer's instructions and primers listed in Suppl. Table 2. The resulting plasmids listed in Suppl. Table 3 were confirmed by DNA sequencing and by Western blot analyses for synthesis of SopB-HA by STM harboring respective plasmids after subculture in LB for induction of SPI1. Strains expressing HA-tagged mutant *sopB* alleles were generated by λ Red-mediated allelic exchange as described (Hoffmann et al., 2017). Briefly, strain MvP2726 was generated by replacing *sopB* by a targeting DNA cassette TC1 generated from pWRG717 using primers sopB In717 For and sopB In717 Rev2 (see Suppl. Table 1 and 2). Insertion of the cassette was controlled by check PCR with sopB DelCheck Rev and k1 RedDel. MvP2726 was used as parental strain for a second λ Red-mediated recombination with TC2 for exchange of the *sopB* locus against wt or mutant alleles. TC2 DNA was generated from plasmids (Suppl. Table 3) with wt or mutant alleles of *sopB*::HA using primers SeqFor and sopB-HA RedIn Rev (Suppl. Table 2). Mutant strains with successful allelic exchange of the *sopB* locus were cured from helper plasmid pWRG730, and synthesis

of SopB was controlled by Western blot alleles of *S.* Typhimurium strains after culture under SPI1-inducing conditions. In Western blots, the HA tag was detected using rat anti-HA monoclonal antibodies (clone 3F10, Roche 11867423001). For generation of a 3xFLAG-tagged allele of *sopB*, the *sopB* locus of strain MD1163 was transferred to ATCC14028 by P22 transduction (Suppl. Table 1).

Ethics statement

All animal experiments were performed in compliance with the German animal protection law (TierSchG) and approved by the local animal welfare committee (Niedersachsische Landesamt für Verbraucherschutz und Lebensmittelsicherheit Oldenburg, Germany; Landesamt für Natur, Umwelt und Verbraucherschutz, North Rhine Westfalia) under the code 84-02.04.2017.A397 and 84–02.04.2021.A043 including all approved changes.

***In vivo* infection experiments**

Adult C57BL/6J wild type mice, *Casp1*$^{-/-}$ (B6. 129S2-Casp1^{tm1Flv}/J, stock no.016621), *Asc*$^{-/-}$ mice (B6. 129-Pycard^{tm1Vmd}), and *Tnfrsf1a*$^{-/-}$ (Tnfrsf1a^{tm1MAK}; stock 002818) were obtained from Jackson Laboratory (Bar Harbour, USA) and bred locally at University Hospital RWTH Aachen under SPF conditions. *Mlkl*$^{-/-}$ (BV6. 129-Mlkl$^{tm1/J}$), and *Casp8*$^{\Delta IEC}$ (B6. 129-Casp8^{tm1Hed}/J; stock 027002) mice were provided by James Murphy (Walter and Eliza Hall Institute of Medical Research, Australia) and Claudia Günther (University Hospital Erlangen, Germany) and bred locally at University Hospital RWTH Aachen under SPF conditions. Overnight bacterial cultures grown on a shaker in Luria Bertani (LB) were diluted 1:10 and incubated at 37°C on a wheel (22 rpm) under mild aeration to induce SPI1 T3SS activity until reaching the logarithmic phase (OD_{600}: 0.5) as described (Barthel et al., 2003; Zhang et al., 2014). Bacteria were washed and diluted to obtain the appropriate inoculum in PBS. One-day-old animals were orally infected with 100 CFU *S.* Typhimurium. 9-week-old adult female mice

were pretreated with streptomycin (20 mg) administered by intragastric gavage one day prior to oral infection with 10^7 CFU *S.* Typhimurium, as previously described (Barthel et al., 2003). At the indicated time point postinfection (p.i.), liver, spleen and mesenteric lymph nodes (MLN), small intestine as well as blood samples were collected. Viable counts were obtained by serial dilution and plating of homogenised tissue on LB agar plates supplemented with the appropriate antibiotic(s). Small intestinal tissues were collected, fixed in 4% paraformaldehyde (PFA) for histological analysis or processed for total tissue expression, respectively. For *ex vivo* tissue cytokine secretion, small intestines were longitudinally opened and sectioned into smaller pieces. Tissue pieces were incubated in 100 µL RPMI medium supplemented with 10% fetal calf serum (FCS) at 37 °C in a 5% CO_2 humidified atmosphere. After 2 h, 50 µl supernatant was collected and analysed.

Gene expression analysis

RNA was isolated from the epithelial cell pellet or homogenised intestinal tissue using TRIzol® according to manufacturer's recommendations. The RNA concentration was determined using a NanoDrop 1000 spectrophotometer (Thermo Scientific). First-strand complementary DNA (cDNA) was synthesised from 5 µg total RNA using Oligo-dT primers, 5X PCR buffer, dNTP, RevertAid reverse transcriptase and RiboLock RNase inhibitor (ThermoFisher Scientific). RT-PCR was performed using Taqman technology with an absolute QPCR ROX mix (Thermo Scientific). Taqman probes *Hprt* (house-keeping gene, Mm00446968_m1), *Cxcl1* (Mm04207460_m1), *Cxcl2* (Mm00436450_m1), *Cxcl5* (Mm00436451_g1), *Ccl2* (Mm00441242_m1), *Tnf* (Mm00443258_m1), *Reg3g* (Mm00441128_g1), *Bcl2* (Mm01302952_g1) or *Nos2* (Mm00440502_m1) from ThermoFisher Scientific were used. Results were calculated by the $2^{-\Delta\Delta Ct}$ method. Values were normalised to the *Hprt* housekeeping gene and are presented as fold induction over age-matched healthy controls.

204

205 **RNA Seq and transcriptome analysis**

206 RNA was prepared from primary freshly isolated intestinal epithelial cells obtained from age-
207 matched uninfected mice, or mice infected with wt or Δ*sopB S.* Typhimurium at day 1 p.i. using
208 TRIzol®. Libraries were prepared with the QuantSeq 3'mRNA-Seq v2 Library Prep Kit FWD
209 with UDIs (Lexogen), using an input of 125 ng, and were sequenced in single end mode (read
210 1: 75 cycles, index 1: 12 cycles, index 2: 12 cycles, read 2: 0 cycles) on a NovaSeq 6000
211 (Illumina), using a NovaSeq 6000 SP Reagent Kit v1.5 (100 cycles) (Illumina). Raw sequencing
212 reads were trimmed using Cutadapt v4.9 with the following parameters: -j 16 -a "poly
213 A=A(20)" --quality-cutoff 20 -m 20 -u 12, to remove poly-A tails, low-quality bases, and
214 adapter sequences. A genome index was generated using STAR v2.7.11b in genome generation
215 mode (--sjdbOverhang 63) based on the GRCm39.112 mouse reference genome. Trimmed
216 reads were then aligned to the genome index using STAR with parameters --outSAMtype BAM
217 SortedByCoordinate and --quantMode GeneCounts to produce BAM files. Gene-level count
218 matrices were generated using the featureCounts function from the Rsubread package (v2.14.2).
219 Differential gene expression analysis was performed using DESeq2 v1.44.0, including only
220 genes with a total count of at least 60 across all samples. GO enrichment analysis was conducted
221 using the clusterProfiler package (v4.12.6) with the org.Mm.eg.db database. Multiple testing
222 correction was applied using the Benjamini-Hochberg method. GSEA was performed with the
223 python gseapy package (v1.1.9) using genes from the mmu04668 KEGG pathway.

224

225 **Cytokine, chemokine and endotoxin quantification**

226 Cytokine and chemokine levels including the concentrations of TNF and IL-18 in the medium
227 supernatants and serum samples were measured using the LEGENDplex™ Mouse Virus
228 Response Panel (BioLegend, Cat No 740622) and LEGENDplex™ Mouse M1 Macrophage
229 Panel (BioLegend, Cat. Nr 740848) according to the manufacturer's protocol. Samples were

measured using a BD FACS Canto II and analysed with the LEGENDplex™ Data Analysis Software Suite (Qonit). Results are expressed as picograms per milliliter. The heat map was generated using Heatmapper (http://www.heatmapper.ca) (Babicki et al., 2016). CXCL2 secretion by m-IC_{cl2} cells was quantified using a CXCL2 ELISA from Biosite (Cat. No.: PPE 21335). The endotoxin concentration in cell culture medium was measured using the Kinetic-QCL™ Kinetic chromogenic LAL assay (Lonza, Cat. No.: 50-650).

Intestinal epithelial and immune cell isolation and analysis

Primary small intestinal epithelial cells were isolated as previously described (Zhang et al., 2014). Briefly, epithelial cells were detached from the underlying tissue in 30 mM EDTA/PBS with strong shaking. To analyse the number of intraepithelial *S.* Typhimurium, one fraction of epithelial cells was treated with 100 µg/mL gentamicin for 1 h at room temperature, washed in PBS and plated in serial dilutions on selective LB agar plates. The other fraction of epithelial cells was stored in Trizol at -80°C for subsequent gene expression analysis. For the isolation of immune cells, Peyers patches and feces were removed, the intestine was opened longitudinally and transferred into 20 ml of HBSS/3% FBS with 2mM EDTA. The intestine was shaken twice at 150 rpm at 37°C for 20 min. After the second incubation the intestine was rinsed with PBS to remove the EDTA. The remaining intestine was enzymatically digested in RPMI (Gibco) containing 30 µg/ml Liberase™ (Roche) and 100 µg/ml DNase (Roche) for 45min shaking at 37°C. Tissue pieces were filtered through a 100 µm nylon cell strainer (BD) to obtain a single cell suspension. Immune cells were separated using a Percoll gradient by centrifugation at 700 x g for 20 min. at room temperature. Cells were stained using the following antibodies CD45-BV510 (Clone 30-F11), CD45-PE Cy7 (Clone 30-F11), Ly6C-PerCPCy5.5 (Clone HK1.4), Ly6G-PE (Clone 1A8), Ly6G-Spark NIR 685 (Clone 1A8), Ly6C-BV711 (HK1.4), CD11b-APC Cy7 (Clone N418), CD11b-BUV 395 (Clone M1/70), CD64-APC (Clone X54-5/7.1), CD64-PE Dazzle (Clone X54-5/7.1), MHCII-AF488 (Clone M5/114.15.2), MHCII-BV510

(Clone M5/114.15.2), PDL1-PE (Clone 10F.952), SiglecF-APCR700 (Clone 90/CD38; BD), Epcam-BV421 (Clone G8.8), CD3-FITC (Clone 17A2), CD19-FITC (Clone 6D5), (Biolegend) and DAPI (Roth) for subsequent analytical flow cytometry. Data were acquired with a BD FACS Canto II and analysed with FlowJo X. For FACS sorting, approximately 3-6 million monocytes, macrophages, and neutrophils were sorted by BD Biosciences FACS Aria Fusion Sorter and directly collected into RNA lysis Buffer (QIAGEN RNeasy Micro Kit QIAGEN). Total RNA of each immune cell population was extracted using QIAGEN RNeasy Micro Kit following manufacturer's instructions.

***Ex vivo* stimulation of isolated immune cells**

Immune cells were collected, washed in 3% FCS/PBS and counted. 10^6 cells were cultured in 500 µL Iscove's modified Dulbecco's medium (Thermo Fisher Scientific) supplemented with 10% FBS, with/without 1 µL of the cell activation cocktail (phorbol myristate acetate (PMA) and ionomycin (I), Biolegend, Cat. No.: 423302). After incubating the cells at 37°C in a 5% CO_2 humidified atmosphere for 1 h, 5 µg/ml brefeldin A (BFA, Biolegend, Cat. No.: 420601) was added. After 3 more hours of re-stimulation, cells were collected, washed once with 3% FCS/PBS, and resuspended in 3% FCS/PBS. Cells were then harvested and stained with the following antibodies (Biolegend): CD45-APCR700 (Clone 30-F11; BD Biosciences), CD3-APCFire750 (Clone 17A2), PDL1-APC (Clone 10F.952), SiglecF-BB515 (Clone E50-2440; BD Biosciences), CD11c-BUV737 (Clone N418: BD Biosciences), CD64-PEDazzle (Clone 90/CD38), CD11b-BV786 (Clone M1/70), F480-PECy5 (Clone BM8), Epcam-BV421 (Clone G8.8), MHCII-BV510 (Clone M5/114.15.2), Ly6C-PerCP-Cy5.5 (Clone HK1.4), Ly6G-BV711 (Clone 1A8), CD80-BUV 805 (Clone 16-10A1; BD Biosciences), CD19-PECy7 (Clone 6D5) for 20 min at 4°C and 30 min with Zombie UV at 4°C (Cat. No.: 423107, BioLegend). Stained cells were fixed and permeabilised (BD Cytofix/Cytoperm™, Cat. No. 554722 according to manufacturer`s instructions) prior to intracellular cytokine staining with a TNFα-

PE (Clone MP6-XT22) antibody overnight at 1:500 dilution (Biolegend). Data were acquired on a Cytek Aurora flow cytometer and analysed with FlowJo X.

Immunostaining

Fixed small intestinal tissues were embedded in paraffin or OCT. 4 μm thick sections were deparaffinised and rehydrated. Slides were stained with haematoxylin and eosin Y solution for H & E staining and observed under a Zeiss Axio Imager M2 light microscope. The thickness of the *lamina propria* as a measure of the tissue oedema was measured using the ZEN 3.4 imaging software. For immunofluorescence staining, tissue sections were blocked with 10% normal donkey serum/5% BSA/PBS. Rabbit anti-Ki67 (Ab15580, Abcam), mouse anti-E-cadherin (610182, BD Transduction Laboratories), rat anti-PMN (Ly6-6B2, SeroTec), rabbit anti-Muc2 (GTX100664, BIOZOL), and rabbit monoclonal anti-ADAM17 (JM10-35, Invitrogen) were used at the appropriate dilution followed by the fluorophore-conjugated donkey secondary antibody (Jackson ImmunoResearch). AF647-conjugated wheat germ agglutinin (WGA, Vector Laboratories, FL1021) was used to visualise the mucus layer. The *in situ* cell death detection Kit (Roche) was used following manufacturer's instructions to detect TUNEL positive cells. Slides were counterstained with DAPI (Vector Laboratories) and images were taken using a Zeiss ApoTome.2 system microscope connected to an Axiocam 506 digital camera (Zeiss). The thickness of the *lamina propria* and the fraction of the $ADAM17^{+}$ intestinal epithelial apical surface were quantified using the ZEN 3.4 imaging software.

Neonatal intestinal epithelial stem cell organoid culture

Neonatal intestinal epithelial stem cell organoids (spheroids) were prepared according to established protocols and grown as cell monolayers (Kayisoglu et al., 2021; Zhang et al., 2024). Briefly, small intestinal crypts were isolated by incubation at 4°C in PBS containing 2 mM EDTA for 5 min. from total neonatal small intestine tissue seeded in Matrigel (356231; BD

Biosciences) into 48-well plates (20 µl of Matrigel per well). Matrigel was polymerised at 37°C for 15 min and 250 µl of ENR basal culture medium (advanced DMEM/F12 medium [12634-028; Gibco] supplemented with penicillin/ streptomycin [15140-122; Gibco], 0.01 M HEPES [15630-056; Gibco], 1× Glutamax [35050-038; Gibco], 1× N2 [17502-048; Gibco], 1× B27 [17504-044; Gibco], 500 mM N-acetylcysteine [A9165; Sigma-Aldrich], 50 µg/ml mouse EGF [PMG8045; Gibco], 100 µg/ml mouse noggin [250-38; PeproTech], and 10% of R-spondin conditioned medium purified from the supernatant of stably transfected HEK293T cells) was added to each well. Medium change was performed every 3 days and organoids were passaged 1:5 after 7 days. To obtain cell monolayers, 4-day-old spherical organoids were trypsinised with TrypLE Express (12605-010; Gibco) filtered and washed by centrifugation. Cells were resuspended in ENRWY medium (ENR medium containing 50% Wnt3a conditioned medium) purified from the supernatant of stably L-Wnt-3A expressing HEK cells and 10 µM RhoK inhibitor Y-27632 (M20999; AbMole Bioscience). 200 µl of the cell suspension was added to each well of a 48-well cell culture plates followed by a 1-min centrifugation step to promote attachment to the Matrigel layer. After 16–18 h, non-adherent cells were removed, and the cells were incubated again at 37°C for 24 h. Dead cells were removed by washing with prewarmed PBS. R-spondin-producing and Wnt3a-producing HEK293T cells were kindly provided by Calvin Kuo (Stanford University, Stanford, CA, USA) and Sina Bartfeld (Berlin Technical University, Berlin, Germany), respectively. Confluent cell monolayers were infected with *S.* Typhimurium at a multiplicity of infection (MOI) of 10:1 for 1 h. Monolayers were washed three times with warm PBS and supplemented with pre-warmed ENRWY media containing 100 µg/mL gentamicin (Sigma) for 1h at 37°C to remove extracellular bacteria. Infected monolayers were washed again three times in warm PBS and lysed. The number of intracellular bacteria was determined by serial dilution and plating on selective LB agar plates. The invasion rate was calculated as (number of intracellular bacteria/number of administered bacteria) X 100[%].

To evaluate the role of secretory autophagy for cytokine release by intestinal stem cell organoids, confluent 2D organoids were washed once with warm PBS prior to infection with *S.* Typhimurium, to remove dead cells. Cells were left untreated or treated with 200nM rapamycin for 1 h. The supernatant was then removed, and the fresh ENRWY media containing 20nM rapamycin was added for subsequent steps. Wt or Δ*sopB S.* Typhimurium was added to stem cell organoid cells grown to confluency at a multiplicity of infection (MOI) of 10:1. After 1 h of infection, infected monolayers were washed three times with warm PBS and supplemented with pre-warmed ENRWY media containing 100 µg/mL gentamicin (Sigma) for 1 h at 37 °C to remove extracellular bacteria. Supernatants were analysed using a cytometric bead array (Cytometric Bead Array Kit, BioLegend) according to the instructions of the manufacturer.

ADAM17 activity assay

Isolated intestinal epithelial cells were washed twice with PBS by centrifugation at 300 x g for 5 min at 4°C. The pellets were resuspended in PBS and transferred to a black 96-well plate suitable for fluorescence measurements. The pellets were incubated at 37°C in a humidified 5% CO_2 incubator for 30, 60, 90, 120 min and 180 min in the presence of 10 µM ADAM17/TACE substrate (Sigma, Cat. Nr: 616407), with or without 10 µM ADAM17/TACE inhibitor (Sigma, GW-3333), in a total volume of 50 µl PBS. ADAM17 enzymatic activity was quantified at the indicated time points by measuring fluorescence intensity at Ex/Em=320 nm/420 nm using a fluorescence microplate reader (SpectraMax i3, ROM v1.4 b18). At the end of the incubation period, IEC pellets were lysed using 0.1% Triton X-100 (Cayman, item: 601172) and total protein concentrations of the lysates were determined using the Bradford assay (Bio-Rad) following the manufacturer's instructions.

m-IC$_{cl2}$ co-culture experiments

m-IC_{cl2} cells were seeded onto polyethylene terephthalate (PET) ThinCert™ transwell inserts with a pore size of 3 µm (Greiner Bio-One, Kremsmünster, Austria) and grown to a confluent monolayer of polarised epithelial cells in m-IC_{cl2} medium supplemented with 2% heat-inactivated FCS for 10–12 days with medium changes three times per week (Bens et al., 1996). The integrity of the epithelial monolayer was assessed by monitoring the transepithelial electrical resistance (TEER). Wild-type (wt) and Δ*sopB S.* Typhimurium were added to the apical compartment at a multiplicity of infection (MOI) of 10:1. To promote host cell contact, plates were centrifuged at 1,200 rpm for 5 min. After 1 h incubation at 37 °C, cell monolayers were washed with warm PBS and incubated in fresh cell culture medium supplemented with 100 µg/ml gentamicin (Sigma, Cat. No.: 1405-41-0) for 1 h to remove extracellular bacteria. After 1 h, the medium was replaced by fresh medium supplemented with 20 µg/ml gentamicin. Non-infected m-IC_{cl2} cells were treated similarly.

Proteomics and phosphoproteomics

m-IC_{cl2} cells were grown to confluency and polarised for 7 days. Cells were infected at a MOI of 10:1 for 1 h and lysed in 1% Triton X-100, 150 mM NaCl, 50 mM Tris-HCl (pH 7.4), 0.5% sodium deoxycholate, and 0.1% SDS including Roche's complete proteinase and phosphatase inhibitors. For the full proteome, 30 µg protein was used and prepared by protein clean up and enzymatic cleavage using a paramagnetic bead approach as described previously (Wang et al., 2021). The only difference was that the samples were not acidified before loading on the beads for protein clean-up. Peptides were eluted in two fractions, the first one with 87% acetonitrile in 10 mM ammonium formate (pH 10, Sigma Aldrich), and the second one with 2% dimethylsulfoxide (DMSO, Sigma Aldrich). Both fractions were analysed using liquid chromatography (LC) coupled to a mass spectrometer (MS). In detail, the peptides were separated on a nano-UPLC system (Ultimate 3000, Dionex, USA) with a trapping column (flow rate 5 µl/min, Acclaim PepMap 100 C18, 3 µm, nanoViper, 75 µm×5 cm, Thermo Fisher,

Germany) and an analytical column (flow rate 0.3 µl/min, Acclaim PepMap 100 C18, 3 µm, nanoViper, 75 µm × 25 cm, Thermo Fisher, Germany) using a 160 min non-linear gradient as described in (Wang et al., 2021). The nano-UPLC system was coupled to the MS (QExactive HF, Thermo Scientific, USA) via a chip-based ESI source (Nanomate, Advion, USA). The only difference compared to the previously described workflow (Wang et al., 2021) was that not the top 10 but the top 15 precursor ions were subjected to MS/MS analysis. The obtained raw data were processed against the UniProtKB reference proteome of *Mus musculus* (March, 18, 2023), using Proteome Discoverer 2.5 and the following parameters: carbamidomethylation as fixed modifications, oxidation of methionine and acetylation of the protein N-terminus as variable modifications. This workflow resulted in information on 4682 proteins.

For the phosphoproteome, 600 µg protein were used, followed by protein clean up and enzymatic cleavage using a paramagnetic bead approach as described previously (Grosskopf et al., 2021). Peptides were eluted after the peptide clean-up in water resulting in one fraction. After elution, a two-step enrichment of phosphorylated peptides using the HighSelect™ TiO2 Phosphopeptide Enrichment Kit (Thermo Scientific, USA) and the High-Select™ Fe-NTA Phosphopeptide Enrichment Kit (Thermo Scientific, USA) was performed as described before (Grosskopf et al., 2021). Enriched phosphorylated peptide samples were analysed using the same LC-MS/MS system as the full proteome samples with a 160 min non-linear gradient and with adjusted MS parameters: precursors between 350 m/z and 1550 m/z were detected at a resolution of 120K. MS1 automatic gain control (AGC) target was set to 3e6, with a maximum injection time of 150 ms. The top 15 precursors were isolated using a window of 0.7 Th, with MS2 AGC target 2e5 and a maximum injection time 150 ms. The normalised collision energy (NCE) was 34, fixed first mass 120 m/z, and MS2 resolution 60K. A dynamic exclusion of 45 s was used. The obtained raw data were processed against the same UniProtKB reference proteome as the proteome, using Proteome Discoverer 2.5 and the following parameters: phosphorylation on serine, threonine, or tyrosine, oxidation of methionine, and acetylation of

the protein N-terminus as variable modifications. This workflow resulted in information on 5242 proteins, 44225 peptide isoforms, and 15018 phosphosites.

For the identification of regulated proteins/phosphosites and enrichment analysis, the data were first filtered for proteins and phosphosites identified at least in three replicates, followed by log2-transformation and median-normalisation. The average Log2(FCs) were calculated, and regulated proteins and phosphosites were determined using the student's t-test. Obtained p-values were adjusted for multiple testing, according to Benjamini & Hochberg. Proteins and sites were considered significantly regulated with FDR≤0.05. Enrichment analyses were conducted with regulated proteins or regulated phosphosites (FDR≤0.05) using Ingenuity Pathway Analysis (IPA, Qiagen). Enrichment p-values were adjusted for multiple testing, according to Benjamini & Hochberg. Pathways were considered significantly enriched with FDR≤0.05.

Affinity enrichment of SopB-associated host proteins

Polarised and confluent cell layers of m-IC_{cl2} cells were infected with wt *S.* Typhimurium or *S.* Typhimurium carrying a chromosomal allele of *sopB* with triple FLAG-tag at a multiplicity of infection (MOI) of 10:1. Plates were centrifuged at 300 x g for 1 min to initiate host cell contact. After 1 h incubation at 37 °C, cell monolayers were washed with cold PBS and lysed in Pierce RIPA buffer (Thermo Scientific) supplemented with cOmpleteTM protease inhibitor tablet (Roche) and PhosSTOP (Roche). The cell lysate was harvested by centrifugation at 13,000 rpm for 20 min at 4°C and mixed with 30 µL of washed anti-FLAG® M2 Affinity Gel (Sigma, A2220). The mixture was rotated at 4°C for 4 h to allow binding. Unbound proteins were washed away with 0.01% PBS-Triton X-100 buffer at 5,000 g for 5 min. at 4°C. The bound proteins were eluted using 150µg/mL FLAG peptide (Waters) prepared in 0.05% RapiGest (Waters). The eluted proteins were resuspended in 50 mM HEPES (pH 8) containing 1% SDS, 40 mM 2-chloroacetamide, and 10 mM TCEP, then incubated at 95°C for 5 min to facilitate

reduction and alkylation. Nucleic acids were digested with Benzonase (2.8 U/Sample) at 37°C for 30 min. Samples were processed for mass spectrometry using a modified SP3 protocol (Hughes et al., 2019). Proteins were digested with Trypsin and LysC at 37°C for 14 h. Peptides were labeled using 6plex TMT (Thermo Fisher) following Zecha et al. (Creskey et al., 2023). Samples were pooled and desalted using a Waters OASIS HLB µElution Plate. LC-MS/MS was performed on an UltiMate 3000 RSLCnano coupled to an Orbitrap Exploris 480 mass spectrometer (Thermo Fisher). Peptides were separated on a C18 analytical column (IonOpticks) over 160 min (1–40% B, 0.25 µl/min). MS1 spectra (400–1,600 m/z) were acquired at 120,000 resolution; the top N precursors (charge 2–5, cycle time 3s) were fragmented (NCE 32) and analysed at 15,000 resolution. Raw files were processed with MSFragger (v3.8) using the *Mus musculus* (UP000000589) and *S.* Typhimurium 14028s (UP000002695) UniProt databases with contaminants and reverse sequences. Downstream analyses, including normalisation and differential expression, were conducted in R (RStudio v2021.09.2) using limma (v3.54.2), vsn (v3.66.0), and the tidyverse suite (dplyr v1.1.1, ggplot2 v3.4.2).

Immunoprecipitation

Affinity purification of SopB-interacting proteins was performed as described above. For immunoblotting of ADAM17, protein eluted from the anti-FLAG® M2 Affinity Gel, total m-IC_{cl2} cell lysate, and *S.* Typhimurium *sopB*::3xFLAG lysate were incubated at 95°C for 10min with 4x SDS loading dye, loaded on a 10% SDS-PAGE, and run at 120V for 60min. Proteins were transferred to a nitrocellulose membrane at 250mA for 90min. The membrane was blocked with 5% milk-TBS-T for 1h at room temperature and incubated with anti-FLAG® M2 antibody diluted 1:2000 (F1804, Sigma) or anti-ADAM17 antibody diluted 1:2000 (JM10-35, Invitrogen) overnight at 4 °C. After washing three times with TBS-T, the membrane was incubated with the secondary antibody conjugated to HRP for 1h at room temperature in 5%

milk-TBS-T. Finally, the washed membrane was incubated with SuperSignal West Femto Maximum Sensitivity Substrate (Thermo Scientific) and scanned using a C-DiGit Blot Scanner (LICORbio).

Network analysis

To identify potential interactions between SopB affinity enriched host proteins and the ADAM17 complex consisting of ADAM17, iRhom1/RHBDF1, iRhom2/RHBDF2, and FRMD8, the curated interactomics database BioGRID was queried. To infer candidate–complex connectivity via direct interactions and shared interactors, we performed high-throughput AlphaFold-Multimer (AFM) prediction and interaction confidence scoring (Schmid & Walter, 2025; Schwarz et al., 2025). Protein sequences were retrieved via the UniProt API (UniProt, 2025) using custom Python scripts (Python v3.11.0). Proteins larger than 650 residues were segmented into prediction units using AlphaFold DB–derived pLDDT and PAE profiles to place boundaries in low-confidence regions between structural domains. All pairwise combinations were subjected to AFM prediction (Jumper et al., 2021) using MSAs generated with MMseqs2 (Steinegger & Soding, 2017). For each protein pair, AFM produced five models, which were ranked using the actifpTM score (Varga et al., 2025). A custom pipeline extracted Cα coordinates from both chains and defined interface residue pairs as positions within 10 Å. For each model, the mean interface PAE (iPAE) across all interface residues was computed and transformed to a normalised score by mapping iPAE ≤ 5 Å to 1, iPAE > 15 Å to 0, and linearly scaling intermediate values (5–15 Å). The model interaction score was calculated as the arithmetic mean of actifpTM and iPAE. Pairwise confidence was reported as the mean across the five AFM models (reflecting consensus across AFM weight sets), and high-confidence PPIs for network inclusion were defined as mean interaction confidence > 0.75. In addition, connectivity was augmented using a directed kinase-to-substrate reference database assembled by integrating curated resources: OmniPath (Turei et al., 2016), HPRD (Goel et al., 2012),

PhosphoSitePlus (Hornbeck et al., 2015), Phospho.ELM (Diella et al., 2008), Reactome (Milacic et al., 2024) and DEPOP (Damle & Kohn, 2019). Network construction and visualisation were performed with custom Python scripts; scripts are available upon reasonable request or, after publication, via https://github.com/Clusterbiology.

Statistics

Survival was analysed by log-rank (Mantel -Cox) test. The non-parametric Mann Whitney test was used for the comparative analysis of two groups. The Kruskal-Wallis combined with Dunn's multiple comparison test was employed for the statistical analysis of more than two groups. If data were normally distributed as confirmed using the Shapiro-Wilk test, the student's t-test (two groups) or the one-way ANOVA test with Tukey's posttest (more than two groups) was used. Two-way ANOVA with Sidak or Tukey's multiple comparison test was employed for the statistical analysis of two groups that have been split on two independent variables. Graphpad Prism Software 10 was used for statistical evaluation. Differences were considered significant at $p < 0.05$, *; $p < 0.01$, **; $p < 0.001$, ***; and $p < 0.0001$, ****.

Results

SopB delays disease progression and immune stimulation

In most cases, pathogens with genetic deletions in important virulence factors exhibit an attenuated phenotype. In contrast, infection of newborn mice with a *Salmonella enterica* subsp. *enterica* sv. Typhimurium (*S.* Typhimurium) strain lacking the *Salmonella* pathogenicity island (SPI)1-type 3 secretion system (T3SS) translocated phosphatidyl-inositol phosphatase SopB (Δ*sopB*) resulted in significantly accelerated disease progression and earlier mortality as compared to infection with wildtype (wt) *S.* Typhimurium (Fig. 1a). Complementation (compl.) with *sopB* together with its chaperone *sigE* reversed this phenotype. Despite reports and own *in vitro* evidence for a role of SopB in enterocyte invasion (Suppl. Fig. 1a and b), no difference was observed between the number of intraepithelial Δ*sopB* and wt *S.* Typhimurium bacteria *in vivo* (Fig. 1b and c) or bacterial counts in total mesenteric lymph node, liver and spleen tissue at day 1 and 2 p.i. (Suppl. Fig. 1c and d) (Hernandez et al., 2004; Humphreys et al., 2012; Piscatelli et al., 2016; Zhou et al., 2001). In contrast, intestinal epithelial expression of the chemokines *Cxcl2*, *Cxcl1* and *Ccl2* as well as the antimicrobial protein *Reg3g* was strongly increased at day 1 p.i. with Δ*sopB S.* Typhimurium, whereas it remained unaltered after infection with wt *S.* Typhimurium or with *S.* Typhimurium deficient in the important SPI1-T3SS translocated effector molecule $SopE_2$ (Δ$sopE_2$) (Fig. 1d, Suppl. Fig. 1e). At day 2 p.i. *Cxcl2*, *Cxcl1*, *Ccl2*, *Reg3g* and *Cxcl5* expression also started to increase after wt or Δ$sopE_2$ *S.* Typhimurium infection but was still significantly higher expressed in animals infected with Δ*sopB S.* Typhimurium (Fig. 1e; Suppl. Fig. 1f). Global transcriptome analysis at day 1 p.i. confirmed the increased expression of innate immune genes after Δ*sopB S.* Typhimurium infection (Suppl. Fig. 1g). Also, the systemic immune response was affected. Serum cytokine levels of IFN-γ, TNF-α, and IL-6 as well as chemokine levels of CXCL1, CCL2, and CXCL10

were significantly higher in Δ*sopB* as compared to wt *S.* Typhimurium-infected mice at day 2 p.i. (Fig. 1f; Suppl. Fig. 1h). These results suggest that the SPI1 effector SopB controls the early local immune stimulation, but also the subsequent systemic cytokine response in the neonatal host *in vivo,* reducing disease progression and delaying infection-induced mortality.

SopB abolishes the early recruitment of inflammatory cells and mucosal tissue damage

Consistent with the observed increase in early chemokine expression, the number of monocytes and neutrophilic granulocytes recruited to the mucosal small intestinal tissue and detected by flow cytometry was strongly enhanced at day 2 p.i. with Δ*sopB* as compared to wt *S.* Typhimurium (Fig. 2a and b; Suppl. Fig. 2a), whereas the number of tissue resident macrophages was not altered (Fig. 2c). Consistently, immunostaining of the small intestine revealed enhanced numbers of neutrophilic granulocytes (PMNs) already at day 1 p.i. and even more pronounced at day 2 p.i. (Fig. 2d-f). Histological analysis further demonstrated significant differences in the mucosal tissue architecture between Δ*sopB* and wt *S.* Typhimurium-infected mice. Infection with Δ*sopB* as compared to wt *S.* Typhimurium led to enhanced thickening of the submucosal tissue as a sign for oedema formation (Fig. 3a and b), a reduced $MUC2^+$ signal that in the context of enhanced tissue inflammation most likely is caused by goblet cell depletion and incomplete differentiation of new replacements from progenitors (Fig. 3c-e) (Chan et al., 2013), and elevated numbers of mostly exfoliating $TUNEL^+$ enterocytes suggesting increased epithelial cell death (Fig. 3f and g). In addition, Δ*sopB S.* Typhimurium-infected mice exhibited increased epithelial cell proliferation illustrated by elevated numbers of $Ki67^+$ cells suggesting epithelial repair (Fig. 3h and i). Thus, SopB suppresses early tissue inflammation upon *S.* Typhimurium infection maintaining mucosal tissue integrity and function. Notably, this phenotype was only observed in the neonatal mouse infection model. No increase in early cytokine and chemokine expression, inflammatory cell recruitment, or

disease severity was observed after infection of adult C57BL/6 mice with Δ*sopB S.* Typhimurium ATCC14028 (Suppl. Fig. 3a-f).

SopB inhibits programmed cell death and TNFα-mediated disease progression

SopB has been shown to induce pro-survival signalling suggesting that increased programmed cell death may occur in the absence of SopB with downstream effects on mucosal tissue integrity and inflammation (Cooper et al., 2011; Drecktrah et al., 2005; Knodler et al., 2005; Marcus et al., 2001; Roppenser et al., 2013; Steele-Mortimer et al., 2000). Therefore, we next infected mice impaired in the different cell death pathways, and monitored their survival, intestinal tissue morphology, bacterial organ counts, and epithelial gene expression. The accelerated disease progression and earlier mortality after Δ*sopB versus* wt *S.* Typhimurium infection was less pronounced but still significant in caspase 1 (Casp1)- and ASC-deficient mice, both impaired in the proinflammatory cell death form pyroptosis (Fig. 4a and Suppl. Fig. 4a). Early mortality after Δ*sopB S.* Typhimurium infection was preserved in intestinal epithelial cell-specific caspase 8-deficient (*Casp8*$^{\Delta IEC}$) animals, impaired in extrinsic apoptosis (Fig. 4b) and no significant increase in the expression of the endogenous apoptosis regulator *Bcl2* and the nitric oxide generating protein iNOS (*Nos2*) was observed although a tendency of elevated *Nos2* expression was noted in Δ*sopB S.* Typhimurium-infected wildtype animals (Suppl. Fig. 4b and c) in contrast to what has previously been reported after infection of adult mice (Drecktrah et al., 2005; Ruan et al., 2016). Only *Mlkl*$^{-/-}$ animals impaired in necroptosis infected with Δ*sopB S.* Typhimurium exhibited a significantly prolonged survival (Fig. 4c) and the histological analysis of *Mlkl*$^{-/-}$ mice revealed reduced thickening of the submucosal tissue in Δ*sopB S.* Typhimurium-infected mice (Fig. 4d and e). Importantly, the number of intraepithelial Δ*sopB S.* Typhimurium, the bacterial organ load in the mesenteric lymph nodes and liver, and the epithelial expression of *Cxcl2* mRNA were not significantly altered in the absence of

MLKL, ASC or Caspase 1 at day 2 p.i. (Suppl. Fig. 4d-g). Together, these results suggest that necroptosis and to some degree pyroptosis contribute to the accelerated disease progression and reduced survival after Δ*sopB S.* Typhimurium infection but likely act downstream of the observed early inflammatory response at day 1 p.i. (Hu et al., 2019).

Necroptosis is induced by TNFα and this cytokine has previously been shown to promote *Salmonella*-induced mucosal inflammation prompting us to test the phenotype of TNF receptor 1 (TNFR1) deficient (*Tnfrsf1a*$^{-/-}$) mice after Δ*sopB S.* Typhimurium infection (Hausmann et al., 2021). The Δ*sopB S.* Typhimurium infection-induced tissue thickening of the *lamina propria* at 2 days p.i. was abolished in the absence of TNFR1 (Fig. 4f and g). More importantly, early mortality observed after Δ*sopB S.* Typhimurium infection was absent in *Tnfrsf1a*$^{-/-}$ animals (Fig. 4h). Notably, the bacterial organ load in the intestinal epithelium, mesenteric lymph node and liver tissue was not significantly altered in the absence of TNFR1 at day 2 p.i. (Suppl. Fig. 4d-f). Consistent with a functional role of TNFα, we found that the *Tnf* mRNA concentration was moderately but significantly enhanced in total small intestinal tissue at day 2 p.i. with Δ*sopB S.* Typhimurium (Fig. 4i). Among immune cells, tissue monocytes exhibited a significantly reduced viability both under non-stimulated and PMA/ionomycin stimulated conditions when isolated at day 2 p.i. from Δ*sopB* as compared wt *S.* Typhimurium-infected animals (Fig. 4j, Suppl. Fig. 5a-c). TNFα may therefore be released from monocytes that were pushed to cell death and cell lysis in the inflamed Δ*sopB S.* Typhimurium-infected tissue environment. Consistently, we observed a significantly lower mean fluorescent intensity (MFI) for intracellular TNFα in stimulated monocytes isolated from Δ*sopB* as compared to wt *S.* Typhimurium-infected animals (Fig. 4k, Suppl. Fig. 5d). In addition to the increased *Tnf* mRNA levels in Δ*sopB S.* Typhimurium-infected intestinal tissue, these findings are consistent with an enhanced cytokine release in the absence of SopB. The released TNFα may in turn induce

enterocyte programmed cell death and contribute to the accelerated systemic disease progression after Δ*sopB S.* Typhimurium infection of neonatal mice (Hu et al., 2019).

SopB-mediated suppression of ADAM17 activity and TNFα secretion

Mice infected with Δ*sopB S.* Typhimurium exhibited a strong, up to 100-fold increase in epithelial expression of the chemokine *Cxcl2* as early as at day 1 p.i., whereas no significant difference was noted between uninfected and wt *S.* Typhimurium-infected animals at this early stage of the infection (Fig. 5a). The difference between Δ*sopB* and wt *S.* Typhimurium-infected mice appeared surprisingly strong given the described requirement of enterocyte invasion for immune stimulation and the low number of infected and thus potentially SopB-manipulated enterocytes at this early stage of the infection (Fulde et al., 2021; Zhang et al., 2014). A possible explanation could be the existence of a soluble mediator amplifying the cellular response upon Δ*sopB S.* Typhimurium infection. Indeed, analysis of *Tnfrsf1a*$^{-/-}$ mice revealed that the early increase in epithelial *Cxcl2* expression in Δ*sopB S.* Typhimurium-infected mice at day 1 p.i. was completely dependent on intact TNFα receptor signalling (Fig. 5b). Similarly, almost all genes induced in wildtype mice by Δ*sopB* but not wt *S.* Typhimurium-infected mice (Suppl. Fig. 1g) remained unaltered in *Tnfrsf1a* $^{-/-}$ mice (Suppl. Fig. 6a). Consistently, gene set enrichment analysis (GSEA) of the small intestinal epithelial transcriptome at day 1 p.i. identified an enrichment of genes associated with TNF receptor signalling after Δ*sopB* but not wt *S.* Typhimurium infection (Fig. 5c). These findings suggested the existence of an early wave of TNFα secretion during the first 24 h of infection in addition to the TNFα-mediated tissue destructive effects described at later stages (day 2) of the Δ*sopB S.* Typhimurium infection (Fig. 4). Intestinal epithelial cells and various immune cells have been shown to increase their TNFα expression in response to *Salmonella* infection (Hausmann et al., 2021; Zhang et al., 2024). However, neither enterocytes nor immune cells such as monocytes, macrophages, or

neutrophilic granulocytes isolated from the small intestine exhibited enhanced *Tnfa* mRNA levels at day 1 p.i. with Δ*sopB* as compared to wt *S.* Typhimurium (Fig. 5d-g).

In addition to the transcriptional regulation, TNFα is regulated on the posttranscriptional level by cleavage and release of membrane bound cytokine molecules by the TNFα converting enzyme (TACE), also called a disintegrin and metalloprotease 17 (ADAM17). ADAM17-mediated cleavage is activated by MAPK p38 and ERK (Xu et al., 2012). Moreover, ADAM17-mediated TNFα release is influenced by Cdc42, a known interaction partner of SopB (Endo et al., 2009; Jin et al., 2013). Using a fluorescent ADAM17 reporter in combination with a highly ADAM17-specific pharmacological inhibitor, we were able to detect ADAM17 activity in total intestinal epithelial cells isolated from mice at 1 day p.i. with Δ*sopB* but not wt *S.* Typhimurium (Fig. 5h, Suppl. Fig. 6b). In accordance, we also detected a significantly increased ADAM17^{+} area of the apical plasma membrane of the small intestinal epithelium in mice infected with Δ*sopB* but not wt *S.* Typhimurium by immunostaining (Fig. 5i and j). Consistently, the release of TNFα protein from total small intestinal tissue obtained from mice infected for 1 day with Δ*sopB S.* Typhimurium and incubated for 2 h *in vitro* was significantly higher than the TNFα release from tissue of mice infected for 1 day with wt *S.* Typhimurium (Fig. 5k). Finally, epithelial *Tnfrsf1a* mRNA expression encoding the TNFα receptor 1 (TNFR1) was increased at day 1 p.i. after Δ*sopB* but not wt *S.* Typhimurium infection likely amplifying TNFα-mediated signals (Fig. 5l). Thus, SopB inhibits ADAM17 activation and plasma membrane translocation, the release of TNFα and TNFR1-mediated cell signalling in neonatal mice.

Analysis of the interaction of SopB with host cell processes

Our results demonstrated that SopB manipulates cellular processes that promote early innate immune activation, thus explaining the markedly enhanced inflammatory phenotype of Δ*sopB S.* Typhimurium-infected animals. To obtain a more comprehensive view on SopB-manipulated

cellular processes in enterocytes, we next performed a phosphoproteome analysis of polarized intestinal epithelial m-IC_{cl2} cells infected for 1 h at a MOI of 10 with wt, Δ*sopB* or Δ*sopB* p*sopB* *sigE* *S.* Typhimurium. The full phosphoproteome (5242 protein groups, 44225 peptide isoforms, 15018 phosphosites) was corrected for changes in protein abundance based on a full proteome (4682 protein groups) and analysed for differentially activated core cell signalling pathways. Beside previously described pathways such as PI3K and Akt signalling, we identified activated ERK/MAPK, JAK/STAT, chemokine and mechanistic target of rapamycin (mTOR) pathways in enterocytes upon infection with *S.* Typhimurium representing potential targets for SopB (Fig. 6a). Additionally, we analysed the transcriptome of total primary intestinal epithelial cells isolated at day 1 p.i., identifying genes with an increased expression in the presence of SopB as compared to its absence (Suppl. Fig. 1g, blue dots). Enriched GO terms representing significantly upregulated genes in animals infected with wt *S.* Typhimurium compared to animals infected with Δ*sopB* *S.* Typhimurium suggested an influence of SopB on autophagy and signalling by the mTOR-containing protein complex TORC1 (Fig. 6b). Notably, three differentially expressed genes, *Rnf152* (ring finger protein 152), *Sesn1* (Sestrin 1) and *Sesn3* (Sestrin 3) control the TORC1 signalling pathway consistent with alterations in the autophagocytotic process in the presence of SopB. Finally, we performed an affinity enrichment screen to identify host proteins directly or indirectly interacting with SopB. Here we used a strain of *S.* Typhimurium chromosomally expressing a triple FLAG-tagged SopB in combination with polarized intestinal epithelial m-IC_{cl2} cells. SopB was purified after 1 h of co-culture to allow SPI1-T3SS-mediated translocation of the tagged SopB into the cell and interaction with host proteins, and co-purified proteins were identified by mass spectrometry. Among other enriched proteins, this screen identified the cytoplasmic linker associated protein (CLASP)1, previously associated with autophagosome trafficking along microtubules (Liao et al., 2025), the cytoplasmic casein kinase 1 epsilon (CSNK1E), and the serine/threonine

phosphatase 2A (PP2A) 56 kDa regulatory subunit beta isoform (PPP2R5B), involved in regulation of the major serine/threonine phosphatase PP2A (Neisch et al., 2017) (Fig. 6c).

Next, we used the AlphaFold Multimer (AFM) pipeline to predict potential interactions between proteins identified in our SopB affinity enrichment screen (SopB interactome, Fig. 6c) and known proteins of the ADAM17 complex, ADAM17, iRhom1/RHBDF1, iRhom2/RHBDF2, and FRMD8. Interestingly, this analysis attributed a high confidence score to interactions between the identified SopB interactome protein CSNK1E and ADAM17 as well as between the identified SopB interactome protein PP2R5B and ADAM17 or iRhom2/RHBDF2 (Fig. 6d, results of all tested pairwise combinations shown in Suppl. Fig. 6c). No direct interaction was detected between SopB and ADAM17 (Suppl. Fig. 6d). Therefore, we next generated an integrated network connecting proteins of the SopB interactome (Fig. 6c) and kinases identified in the phosphoproteome approach (Fig. 6a) together with ADAM17 complex members using an AFM-augmented protein-protein interaction (PPIs) approach with an interaction confidence of > 0.75 and curated kinase-substrate links from public databases. This network visualised some direct and many indirect interactions, consistent with the observed influence of SopB on ADAM17 activity (Fig. 6e).

Besides its effect on ADAM17 activity, the phosphoproteome and transcriptome analyses indicated an influence of SopB on mTOR-regulated autophagy. Secretory autophagy represents a non-canonical secretion pathway and uses the autophagy machinery and autophagosomal transport to release cytokines without signal peptide such as IL-18 (Blommaart et al., 1995; Weigert & Herhaus, 2024). Consistent with enhanced secretory autophagy in intestinal epithelial stem cell organoids infected with Δ*sopB* as compared to wt *S.* Typhimurium, we found that the release of IL-18 but not IL-6 protein was increased (Fig. 6f and g). Importantly, this IL-18 release was reduced to levels observed after wt *S.* Typhimurium infection by pretreatment with the mTOR inhibitor rapamycin (Fig. 6f). Also, the release of IL-18 protein from small intestinal tissue obtained from mice infected with Δ*sopB S.* Typhimurium for 1 day

and incubated *in vitro* for 2 h was significantly higher than the IL-18 release from intestinal tissue of mice infected with wt *S.* Typhimurium (Fig. 6h). In contrast, no influence of SopB on the secretion of the chemokine CXCL2 or release of the innate immune stimulus lipopolysaccharide (LPS) from *S.* Typhimurium-infected epithelial cells was observed (Suppl. Fig. 6e and f). Thus, SopB interferes with cellular processes such as ADAM17-mediated TNFα secretion and the release of cytokines such as IL-18 by secretory autophagy to suppress the early inflammatory response in the neonatal host.

The N-terminal domain of SopB mediates early immune suppression

SopB features functionally distinct N- and C-terminal domains. The C-terminal domain is well known to exert phosphatidylinositol phosphatase and phosphotransferase activity (Marcus et al., 2001; Norris et al., 1998; Piscatelli et al., 2016). Mice infected with *S.* Typhimurium mutants with a chromosomal C460S or K528A mutation in SopB that abolish the C-terminally encoded phosphatase activity exhibited a wildtype-like or even protracted disease course and reduced early mortality (Fig. 7a and b). The N-terminal CRIB like motif (aa117-168) interacts with the small GTPase of the Rho family Cdc42 (Burkinshaw et al., 2012; Rogers et al., 2008) and a L76P point mutation in SopB was shown to ablate this interaction, while preserving the phosphatase activity (Rodriguez-Escudero et al., 2011). Mice infected with *S.* Typhimurium carrying this chromosomal L76P point mutation in the N-terminal domain of SopB exhibited a significantly accelerated disease course and earlier mortality reminiscent of Δ*sopB S.* Typhimurium infected animals (Fig. 7c). The bacterial load in total intestinal epithelial cells and liver tissue did not differ between mice infected with Δ*sopB* and $sopB^{L76P}$ *S.* Typhimurium (Suppl. Fig. 7a and b). In addition, infection of neonate mice with either L76P mutant *S.* Typhimurium or Δ*sopB S*. Typhimurium resulted in enhanced expression of the chemokines *Cxcl1*, *Cxcl2* and *Ccl2* at day 1 p.i. and strongly increased tissue infiltration by neutrophils and monocytes at day 2 p.i. (Fig. 7d-h, Suppl. Fig. 7c). Thus, the observed suppression of early

731 immune activation and tissue inflammation in the neonatal host is mainly mediated by functions

732 of the N-terminal domain of SopB.

Discussion

Using our neonatal mouse infection model we here describe the potent immunosuppressive effect of the *S.* Typhimurium SPI1 T3SS translocated effector SopB that completely blunts early chemokine expression and tissue inflammation *in vivo*. Whereas SopB has been shown to synergise with SopE/SopE$_2$ contributing to actin remodelling, ruffle formation, cell invasion, inhibition of lysosomal fusion, and intracellular growth our findings show no influence on enterocyte invasion and intraepithelial survival but suggest that its primary role *in vivo* is the suppression of the early inflammatory host response (Bakowski et al., 2010; Brooks et al., 2017; Chatterjee et al., 2023; Hanisch et al., 2011; Hernandez et al., 2004; Humphreys et al., 2012; Jolly et al., 2014; Liebl et al., 2017; Norris et al., 1998; Piscatelli et al., 2016; Terebiznik et al., 2002; Truong et al., 2018; Zhang et al., 2018; Zhao et al., 2023; Zhou et al., 2001). Suppression of the early host response is generally consistent with the previously described cell survival promoting activity of SopB by Akt stimulation (Cooper et al., 2011; Finn et al., 2017; Knodler et al., 2005; Marcus et al., 2001; Rogers et al., 2008; Roppenser et al., 2013; Steele-Mortimer et al., 2000). The SopB-induced prolonged host survival most likely increases pathogen shedding enhancing the likelihood of transmission in accordance with the presence of the *sopB* gene in all clinical isolates (Hu et al., 2019; Prager et al., 2000).

SopB blunted epithelial chemokine expression and immune cell recruitment at day 1 and markedly reduced it on day 2 after oral infection. This is consistent with the early and sustained detection of SopB and its activity in mucosal tissue *in vivo* (Drecktrah et al., 2005; Giacomodonato et al., 2011; Knodler et al., 2005). Previous reports on the immunosuppressive role of SopB using the *S.* Typhimurium strain SL1344 in the adult mouse model have revealed somewhat contradictory results. One study showed no difference in the degree of colonic tissue edema and PMN infiltration comparing Δ*sopB* with wt *S.* Typhimurium infection, whereas another study demonstrated enhanced colitis severity, goblet cell loss and bacterial

translocation after infection with Δ*sopB S.* Typhimurium (Hapfelmeier et al., 2004; Hu et al., 2017; Hu et al., 2019). Infection of bovine ileal loops with a Δ*sopB* mutant *S.* Dublin strain led to lower tissue infiltration of PMNs (Galyov et al., 1997). Our own analysis of adult mice after infection with Δ*sopB S.* Typhimurium ATCC14028 did not reveal an immunosuppressive role of SopB. Thus, the immunomodulatory phenotype of SopB appears to be particularly strong in the neonatal infection model, possibly due to age-dependent differences in the mucosal immune homeostasis or the small intestine as primary target organ in the neonatal infection model (Zhang et al., 2014; Zhang et al., 2018).

SopB has been well characterised as phosphatidyl-inositol phosphatase mediated by its C-terminal domain (Marcus et al., 2001; Norris et al., 1998; Zhou et al., 2001). This activity alters the phosphorylation status of phosphatidyl-inositol residues at the plasma membrane entry site to activate N-WASP and F-actin polymerisation (Feng et al., 2001; Mallo et al., 2008; Mason et al., 2007; Piscatelli et al., 2016). It has been linked to actin reorganisation and invasion (Piscatelli et al., 2016; Truong et al., 2018; Zhou et al., 2001), membrane fission (Terebiznik et al., 2002), inhibition of lysosomal fusion (Bakowski et al., 2010), ion flux alterations and fluid loss (Mason et al., 2007), as well as early Akt signalling, and host cell survival (Cooper et al., 2011; Drecktrah et al., 2005; Knodler et al., 2005; Marcus et al., 2001; Roppenser et al., 2013; Steele-Mortimer et al., 2000). We did not observe impaired enterocyte invasion and, consistently, two point mutations (C460S and K528A) within the C-terminal domain of SopB known to abolish the phosphatase activity had no significant influence on the course of the disease in neonatal mice (Marcus et al., 2001; Norris et al., 1998; Piscatelli et al., 2016). More recently, the CRIB-like motif of the N-terminal domain of SopB was shown to interact with Cdc42 (Burkinshaw et al., 2012; Rodriguez-Escudero et al., 2011; Rodriguez-Escudero et al., 2006; Rogers et al., 2008). SopB here acts like a guanosine dissociation inhibitor (GDI) maintaining the small Rho GTPase Cdc42 in an inactive state (Burkinshaw et al., 2012).

Cdc42 has been shown to control ADAM17 activity in endothelial cells (Jin et al., 2013). Consistent with an inhibitory effect of SopB on Cdc42, ADAM17 activity and TNFα release were increased in primary epithelial cells and intestinal tissue from Δ*sopB* but not wt *S.* Typhimurium-infected animals. The potent effect of ADAM17 on TNFα release and local and systemic inflammation *in vivo* was illustrated using ADAM17 deficient animals (Horiuchi et al., 2007). Our affinity enrichment screen of SopB interacting host proteins suggested that SopB does not directly interact with ADAM17 but binds for example the host protein phosphatase cofactor PPP2R5B and the kinase CSNK1E to act on ADAM17 or the inflammatory ADAM17 co-factor iRhom2/RHBDF2 influencing TNFα release. Clearly, the suggested direct and indirect molecular interactions between molecules of the SopB interactome and the ADAM17 complex warrant further investigations. Nevertheless, this interaction and the early TNFα release in the absence of SopB could explain the requirement of TNFR1 signalling on epithelial chemokine expression at day 1 p.i. with Δ*sopB S.* Typhimurium. Additionally, Cdc42 influences transcriptional cytokine regulation and thus the SopB-Cdc42 interaction may also contribute to the lower chemokine transcription at day 2 p.i. (Shouib & Eitzen, 2022). Other soluble mediators such as IL-18 may synergise with TNFα and amplify the early inflammatory reaction in the absence of SopB.

Despite a moderate signal strength, both our phosphoproteome analysis and affinity enrichment screen of SopB interacting host proteins *in vitro* and the global transcriptome analysis of the intestinal epithelium *in vivo* indicated a direct or indirect influence of SopB on mTOR, autophagosome function and trafficking. This influence could at least partly be explained by the known interaction of SopB with Cdc42 and the reported stimulatory effect of Cdc42 on mTOR (Burkinshaw et al., 2012; Endo et al., 2009). mTOR is a component of the TORC1 complex that inhibits the initiation of autophagy through direct phosphorylation of the Unc-51-like autophagy activating kinase (ULK)1 (Kim et al., 2011; Ravikumar et al., 2004). Secretory

809 autophagy is an unconventional protein secretion (UPS) pathway allowing the release of
810 leaderless mediators such as IL-18 and IL-1β (Weigert & Herhaus, 2024). Consistent with a
811 role of mTOR-induced secretory autophagy during early tissue inflammation, we found
812 rapamycin-dependent IL-18 secretion by intestinal epithelial stem cell organoids and enhanced
813 IL-18 release from primary intestinal tissue after Δ*sopB* but not wt *S.* Typhimurium infection.
814 Together, our findings reveal a pronounced immunosuppressive effect of SopB in the neonatal
815 *S.* Typhimurium infection model *in vivo*. This activity was independent of the phosphatidyl-
816 inositol phosphatase activity of the C-terminal domain of SopB but required an intact N-
817 terminal domain. Mechanistically, SopB abolished early local tissue inflammation by reducing
818 ADAM17-mediated TNFα release and by inhibiting IL-18 secretion by mTOR-dependent
819 secretory autophagy. SopB thereby delayed disease progression and inflammation-induced
820 mucosal tissue disturbance prolonging host survival.
821

Data availability

The mass spectrometry proteomics data have been deposited to the ProteomeXchange Consortium via the PRIDE partner repository with the dataset identifier PXD045931 and 10.6019/PXD045931 (Perez-Riverol et al., 2025). Transcriptomic data have been deposited at GEO with the accession number GSE300992 (GSM9073322-GSM9073332) and GSE326693. Both datasets are openly accessible. The network construction and visualization Python scripts are available via https://github.com/Clusterbiology.

Author contributions statement

N.D., K.Z., M.W.H. contributed to the conception and design of the work; N.D., C.H.Y., E-L.S., M.B., S.D., M.S., J.P., K.N.F., I.K., K.S., J.D., M.V., T.L., N.T., A.L., A.D., J.S., M.v B., M.H., and K.Z. contributed to the acquisition, analysis, or interpretation of data; S.D. created of new software used in the work; K.Z. and M.W.H. drafted the work. All authors approved and revised the submitted version of the manuscript.

Acknowledgement

We thank Regina Holland, Martina Leufgens, Simone Martin, Josefine Weber-Heynemann, Monika Nietschke, and Ursula Krehe for excellent technical assistance, as well as Narasimha Murthy Keshava Prasad Gubbi for bioinformatic support. This work was supported by the Flow Cytometry Facility, the Immunohistochemistry Facility, the Genomics Facility, and the Transgenic Facility, core facilities of the interdisciplinary Center for Clinical Research (IZKF) Aachen within the Faculty of Medicine at RWTH Aachen University. Financial support was provided by the Priority Program SPP2225 (project ID P446460159, Ho2236/18-1 project to M.W.H. and project ID 446414114, HE1964/23-2 project to M.H.), a research grant (project ID 279874820, LU1360/3-2 to T.L.), the Collaborative Research Centers CRC1382 (project ID 403224013-SFB 1382 project B01, and A05 to M.W.H., M.v.B.), CRC/TRR 359 (project ID

491676693-SFB/TRR359 project A01 to M.W.H.) and CRC1557 (project ID 467522186, SFB1557 project P8 to M.H.) from the German Research Foundation (DFG), the project 'Microbial Stargazing – Erforschung von Resilienzmechanismen von Mikroben und Menschen' (project ID 01KX2324, to N.T.) from the Federal Ministry of Research, Technology and Space (to N.T.), a research grant (project ID 70114893 to M.V.) from the German Cancer Aid, a research grant from the Federal Ministry for Research, Technology and Space, BMFTR (project ID 01KD2435 to S.D.), and the ERC Advanced Grant EarlyLife (project ID: 101019157 to M.W.H.) from the European Research Council. This research project was additionally funded by the START-Program of the Faculty of Medicine at RWTH Aachen University.

References

Aleman, A., Rodriguez-Escudero, I., Mallo, G. V., Cid, V. J., Molina, M., & Rotger, R. (2005). The amino-terminal non-catalytic region of Salmonella typhimurium SigD affects actin organization in yeast and mammalian cells. *Cell Microbiol*, *7*(10), 1432-1446. https://doi.org/10.1111/j.1462-5822.2005.00568.x

Babicki, S., Arndt, D., Marcu, A., Liang, Y., Grant, J. R., Maciejewski, A., & Wishart, D. S. (2016). Heatmapper: web-enabled heat mapping for all. *Nucleic Acids Res*, *44*(W1), W147-153. https://doi.org/10.1093/nar/gkw419

Bakowski, M. A., Braun, V., Lam, G. Y., Yeung, T., Heo, W. D., Meyer, T., Finlay, B. B., Grinstein, S., & Brumell, J. H. (2010). The phosphoinositide phosphatase SopB manipulates membrane surface charge and trafficking of the Salmonella-containing vacuole. *Cell Host Microbe*, *7*(6), 453-462. https://doi.org/10.1016/j.chom.2010.05.011

Barthel, M., Hapfelmeier, S., Quintanilla-Martinez, L., Kremer, M., Rohde, M., Hogardt, M., Pfeffer, K., Russmann, H., & Hardt, W. D. (2003). Pretreatment of mice with streptomycin provides a Salmonella enterica serovar Typhimurium colitis model that allows analysis of both pathogen and host. *Infect Immun*, *71*(5), 2839-2858. https://doi.org/10.1128/IAI.71.5.2839-2858.2003

Bens, M., Bogdanova, A., Cluzeaud, F., Miquerol, L., Kerneis, S., Kraehenbuhl, J. P., Kahn, A., Pringault, E., & Vandewalle, A. (1996). Transimmortalized mouse intestinal cells (m-ICc12) that maintain a crypt phenotype. *Am J Physiol*, *270*(6 Pt 1), C1666-1674. https://doi.org/10.1152/ajpcell.1996.270.6.C1666

Blommaart, E. F., Luiken, J. J., Blommaart, P. J., van Woerkom, G. M., & Meijer, A. J. (1995). Phosphorylation of ribosomal protein S6 is inhibitory for autophagy in isolated rat hepatocytes. *J Biol Chem*, *270*(5), 2320-2326. https://doi.org/10.1074/jbc.270.5.2320

Brooks, A. B., Humphreys, D., Singh, V., Davidson, A. C., Arden, S. D., Buss, F., & Koronakis, V. (2017). MYO6 is targeted by Salmonella virulence effectors to trigger PI3-kinase signaling and pathogen invasion into host cells. *Proc Natl Acad Sci U S A*, *114*(15), 3915-3920. https://doi.org/10.1073/pnas.1616418114

Burkinshaw, B. J., Prehna, G., Worrall, L. J., & Strynadka, N. C. (2012). Structure of Salmonella effector protein SopB N-terminal domain in complex with host Rho GTPase Cdc42. *J Biol Chem*, *287*(16), 13348-13355. https://doi.org/10.1074/jbc.M111.331330

Chan, J. M., Bhinder, G., Sham, H. P., Ryz, N., Huang, T., Bergstrom, K. S., & Vallance, B. A. (2013). CD4+ T cells drive goblet cell depletion during Citrobacter rodentium infection. *Infect Immun*, *81*(12), 4649-4658. https://doi.org/10.1128/IAI.00655-13

Chatterjee, R., Chaudhuri, D., Setty, S. R. G., & Chakravortty, D. (2023). Deceiving the big eaters: Salmonella Typhimurium SopB subverts host cell xenophagy in macrophages via dual mechanisms. *Microbes Infect*, *25*(6), 105128. https://doi.org/10.1016/j.micinf.2023.105128

Cooper, K. G., Winfree, S., Malik-Kale, P., Jolly, C., Ireland, R., Knodler, L. A., & Steele-Mortimer, O. (2011). Activation of Akt by the bacterial inositol phosphatase, SopB, is wortmannin insensitive. *PLoS One*, *6*(7), e22260. https://doi.org/10.1371/journal.pone.0022260

Creskey, M., Li, L., Ning, Z., Fekete, E. E., Mayne, J., Walker, K., Ampaw, A., Ben, R., Zhang, X., & Figeys, D. (2023). An economic and robust TMT labeling approach for high throughput proteomic and metaproteomic analysis. *Proteomics*, *23*(21-22), e2200116. https://doi.org/10.1002/pmic.202200116

905 Damle, N. P., & Kohn, M. (2019). The human DEPhOsphorylation Database DEPOD: 2019
906 update. *Database (Oxford)*, *2019*. https://doi.org/10.1093/database/baz133
907 Das, R., Haque, M. A., Chisti, M. J., Ahmed, T., & Faruque, A. S. G. (2021). Nontyphoidal
908 Salmonella among Children under 5 Years Old in Sub-Saharan Africa and South Asia in
909 the Global Enteric Multicenter Study. *Am J Trop Med Hyg*, *106*(2), 504-512.
910 https://doi.org/10.4269/ajtmh.21-0762
911 Diella, F., Gould, C. M., Chica, C., Via, A., & Gibson, T. J. (2008). Phospho.ELM: a database of
912 phosphorylation sites--update 2008. *Nucleic Acids Res*, *36*(Database issue), D240-244.
913 https://doi.org/10.1093/nar/gkm772
914 Drecktrah, D., Knodler, L. A., Galbraith, K., & Steele-Mortimer, O. (2005). The Salmonella SPI1
915 effector SopB stimulates nitric oxide production long after invasion. *Cell Microbiol*,
916 *7*(1), 105-113. https://doi.org/10.1111/j.1462-5822.2004.00436.x
917 Endo, M., Antonyak, M. A., & Cerione, R. A. (2009). Cdc42-mTOR signaling pathway controls
918 Hes5 and Pax6 expression in retinoic acid-dependent neural differentiation. *J Biol*
919 *Chem*, *284*(8), 5107-5118. https://doi.org/10.1074/jbc.M807745200
920 Feng, Y., Wente, S. R., & Majerus, P. W. (2001). Overexpression of the inositol phosphatase
921 SopB in human 293 cells stimulates cellular chloride influx and inhibits nuclear mRNA
922 export. *Proc Natl Acad Sci U S A*, *98*(3), 875-879.
923 https://doi.org/10.1073/pnas.98.3.875
924 Finn, C. E., Chong, A., Cooper, K. G., Starr, T., & Steele-Mortimer, O. (2017). A second wave of
925 Salmonella T3SS1 activity prolongs the lifespan of infected epithelial cells. *PLoS*
926 *Pathog*, *13*(4), e1006354. https://doi.org/10.1371/journal.ppat.1006354
927 Fulde, M., van Vorst, K., Zhang, K., Westermann, A. J., Busche, T., Huei, Y. C., Welitschanski,
928 K., Froh, I., Pagelow, D., Plendl, J., Pfarrer, C., Kalinowski, J., Vogel, J., Valentin-
929 Weigand, P., Hensel, M., Tedin, K., Repnik, U., & Hornef, M. W. (2021). SPI2 T3SS
930 effectors facilitate enterocyte apical to basolateral transmigration of Salmonella-
931 containing vacuoles in vivo. *Gut Microbes*, *13*(1), 1973836.
932 https://doi.org/10.1080/19490976.2021.1973836
933 Galyov, E. E., Wood, M. W., Rosqvist, R., Mullan, P. B., Watson, P. R., Hedges, S., & Wallis, T.
934 S. (1997). A secreted effector protein of Salmonella dublin is translocated into
935 eukaryotic cells and mediates inflammation and fluid secretion in infected ileal
936 mucosa. *Mol Microbiol*, *25*(5), 903-912. https://doi.org/10.1111/j.1365-
937 2958.1997.mmi525.x
938 Giacomodonato, M. N., Sarnacki, S. H., Llana, M. N., & Cerquetti, M. C. (2011). SopB effector
939 protein of Salmonella Typhimurium is translocated in mesenteric lymph nodes during
940 murine salmonellosis. *FEMS Microbiol Lett*, *317*(1), 100-106.
941 https://doi.org/10.1111/j.1574-6968.2011.02217.x
942 Goel, R., Harsha, H. C., Pandey, A., & Prasad, T. S. (2012). Human Protein Reference Database
943 and Human Proteinpedia as resources for phosphoproteome analysis. *Mol Biosyst*,
944 *8*(2), 453-463. https://doi.org/10.1039/c1mb05340j
945 Grosskopf, H., Walter, K., Karkossa, I., von Bergen, M., & Schubert, K. (2021). Non-Genomic
946 AhR-Signaling Modulates the Immune Response in Endotoxin-Activated Macrophages
947 After Activation by the Environmental Stressor BaP. *Front Immunol*, *12*, 620270.
948 https://doi.org/10.3389/fimmu.2021.620270
949 Hanisch, J., Kolm, R., Wozniczka, M., Bumann, D., Rottner, K., & Stradal, T. E. (2011).
950 Activation of a RhoA/myosin II-dependent but Arp2/3 complex-independent pathway
951 facilitates Salmonella invasion. *Cell Host Microbe*, *9*(4), 273-285.
952 https://doi.org/10.1016/j.chom.2011.03.009

953 Hapfelmeier, S., Ehrbar, K., Stecher, B., Barthel, M., Kremer, M., & Hardt, W. D. (2004). Role
954 of the Salmonella pathogenicity island 1 effector proteins SipA, SopB, SopE, and
955 SopE2 in Salmonella enterica subspecies 1 serovar Typhimurium colitis in
956 streptomycin-pretreated mice. *Infect Immun*, *72*(2), 795-809.
957 https://doi.org/10.1128/IAI.72.2.795-809.2004
958 Hausmann, A., Felmy, B., Kunz, L., Kroon, S., Berthold, D. L., Ganz, G., Sandu, I., Nakamura, T.,
959 Zangger, N. S., Zhang, Y., Dolowschiak, T., Fattinger, S. A., Furter, M., Muller-Hauser,
960 A. A., Barthel, M., Vlantis, K., Wachsmuth, L., Kisielow, J., Tortola, L., . . . Hardt, W. D.
961 (2021). Intercrypt sentinel macrophages tune antibacterial NF-kappaB responses in
962 gut epithelial cells via TNF. *J Exp Med*, *218*(11).
963 https://doi.org/10.1084/jem.20210862
964 Hernandez, L. D., Hueffer, K., Wenk, M. R., & Galan, J. E. (2004). Salmonella modulates
965 vesicular traffic by altering phosphoinositide metabolism. *Science*, *304*(5678), 1805-
966 1807. https://doi.org/10.1126/science.1098188
967 Hoffmann, S., Schmidt, C., Walter, S., Bender, J. K., & Gerlach, R. G. (2017). Scarless deletion
968 of up to seven methyl-accepting chemotaxis genes with an optimized method
969 highlights key function of CheM in Salmonella Typhimurium. *PLoS One*, *12*(2),
970 e0172630. https://doi.org/10.1371/journal.pone.0172630
971 Horiuchi, K., Kimura, T., Miyamoto, T., Takaishi, H., Okada, Y., Toyama, Y., & Blobel, C. P.
972 (2007). Cutting edge: TNF-alpha-converting enzyme (TACE/ADAM17) inactivation in
973 mouse myeloid cells prevents lethality from endotoxin shock. *J Immunol*, *179*(5),
974 2686-2689. https://doi.org/10.4049/jimmunol.179.5.2686
975 Hornbeck, P. V., Zhang, B., Murray, B., Kornhauser, J. M., Latham, V., & Skrzypek, E. (2015).
976 PhosphoSitePlus, 2014: mutations, PTMs and recalibrations. *Nucleic Acids Res*,
977 *43*(Database issue), D512-520. https://doi.org/10.1093/nar/gku1267
978 Hu, G. Q., Song, P. X., Chen, W., Qi, S., Yu, S. X., Du, C. T., Deng, X. M., Ouyang, H. S., & Yang,
979 Y. J. (2017). Cirtical role for Salmonella effector SopB in regulating inflammasome
980 activation. *Mol Immunol*, *90*, 280-286.
981 https://doi.org/10.1016/j.molimm.2017.07.011
982 Hu, G. Q., Yang, Y. J., Qin, X. X., Qi, S., Zhang, J., Yu, S. X., Du, C. T., & Chen, W. (2019).
983 Salmonella Outer Protein B Suppresses Colitis Development via Protecting Cell From
984 Necroptosis. *Front Cell Infect Microbiol*, *9*, 87.
985 https://doi.org/10.3389/fcimb.2019.00087
986 Hughes, C. S., Moggridge, S., Muller, T., Sorensen, P. H., Morin, G. B., & Krijgsveld, J. (2019).
987 Single-pot, solid-phase-enhanced sample preparation for proteomics experiments.
988 *Nat Protoc*, *14*(1), 68-85. https://doi.org/10.1038/s41596-018-0082-x
989 Humphreys, D., Davidson, A., Hume, P. J., & Koronakis, V. (2012). Salmonella virulence
990 effector SopE and Host GEF ARNO cooperate to recruit and activate WAVE to trigger
991 bacterial invasion. *Cell Host Microbe*, *11*(2), 129-139.
992 https://doi.org/10.1016/j.chom.2012.01.006
993 Jin, Y., Liu, Y., Lin, Q., Li, J., Druso, J. E., Antonyak, M. A., Meininger, C. J., Zhang, S. L., Dostal,
994 D. E., Guan, J. L., Cerione, R. A., & Peng, X. (2013). Deletion of Cdc42 enhances
995 ADAM17-mediated vascular endothelial growth factor receptor 2 shedding and
996 impairs vascular endothelial cell survival and vasculogenesis. *Mol Cell Biol*, *33*(21),
997 4181-4197. https://doi.org/10.1128/MCB.00650-13
998 Jolly, C., Winfree, S., Hansen, B., & Steele-Mortimer, O. (2014). The Annexin A2/p11 complex
999 is required for efficient invasion of Salmonella Typhimurium in epithelial cells. *Cell*
1000 *Microbiol*, *16*(1), 64-77. https://doi.org/10.1111/cmi.12180

Jumper, J., Evans, R., Pritzel, A., Green, T., Figurnov, M., Ronneberger, O., Tunyasuvunakool, K., Bates, R., Zidek, A., Potapenko, A., Bridgland, A., Meyer, C., Kohl, S. A. A., Ballard, A. J., Cowie, A., Romera-Paredes, B., Nikolov, S., Jain, R., Adler, J., . . . Hassabis, D. (2021). Highly accurate protein structure prediction with AlphaFold. *Nature*, *596*(7873), 583-589. https://doi.org/10.1038/s41586-021-03819-2

Kayisoglu, O., Weiss, F., Niklas, C., Pierotti, I., Pompaiah, M., Wallaschek, N., Germer, C. T., Wiegering, A., & Bartfeld, S. (2021). Location-specific cell identity rather than exposure to GI microbiota defines many innate immune signalling cascades in the gut epithelium. *Gut*, *70*(4), 687-697. https://doi.org/10.1136/gutjnl-2019-319919

Kim, J., Kundu, M., Viollet, B., & Guan, K. L. (2011). AMPK and mTOR regulate autophagy through direct phosphorylation of Ulk1. *Nat Cell Biol*, *13*(2), 132-141. https://doi.org/10.1038/ncb2152

Knodler, L. A., Finlay, B. B., & Steele-Mortimer, O. (2005). The Salmonella effector protein SopB protects epithelial cells from apoptosis by sustained activation of Akt. *J Biol Chem*, *280*(10), 9058-9064. https://doi.org/10.1074/jbc.M412588200

LaRock, D. L., Chaudhary, A., & Miller, S. I. (2015). Salmonellae interactions with host processes. *Nat Rev Microbiol*, *13*(4), 191-205. https://doi.org/10.1038/nrmicro3420

Liao, Y., Li, X., Ma, W., Lin, X., Kuang, J., Zheng, X., Li, Z., Qiao, F., Liu, C., Zhou, J., Li, F., Li, R., Kang, B. H., Li, H., & Gao, C. (2025). The plant retromer components SNXs bind to ATG8 and CLASP to mediate autophagosome movement along microtubules. *Mol Plant*, *18*(3), 416-436. https://doi.org/10.1016/j.molp.2024.12.013

Liebl, D., Qi, X., Zhe, Y., Barnett, T. C., & Teasdale, R. D. (2017). SopB-Mediated Recruitment of SNX18 Facilitates Salmonella Typhimurium Internalization by the Host Cell. *Front Cell Infect Microbiol*, *7*, 257. https://doi.org/10.3389/fcimb.2017.00257

Mallo, G. V., Espina, M., Smith, A. C., Terebiznik, M. R., Aleman, A., Finlay, B. B., Rameh, L. E., Grinstein, S., & Brumell, J. H. (2008). SopB promotes phosphatidylinositol 3-phosphate formation on Salmonella vacuoles by recruiting Rab5 and Vps34. *J Cell Biol*, *182*(4), 741-752. https://doi.org/10.1083/jcb.200804131

Marcus, S. L., Wenk, M. R., Steele-Mortimer, O., & Finlay, B. B. (2001). A synaptojanin-homologous region of Salmonella typhimurium SigD is essential for inositol phosphatase activity and Akt activation. *FEBS Lett*, *494*(3), 201-207. https://doi.org/10.1016/s0014-5793(01)02356-0

Mason, D., Mallo, G. V., Terebiznik, M. R., Payrastre, B., Finlay, B. B., Brumell, J. H., Rameh, L., & Grinstein, S. (2007). Alteration of epithelial structure and function associated with PtdIns(4,5)P2 degradation by a bacterial phosphatase. *J Gen Physiol*, *129*(4), 267-283. https://doi.org/10.1085/jgp.200609656

Milacic, M., Beavers, D., Conley, P., Gong, C., Gillespie, M., Griss, J., Haw, R., Jassal, B., Matthews, L., May, B., Petryszak, R., Ragueneau, E., Rothfels, K., Sevilla, C., Shamovsky, V., Stephan, R., Tiwari, K., Varusai, T., Weiser, J., . . . D'Eustachio, P. (2024). The Reactome Pathway Knowledgebase 2024. *Nucleic Acids Res*, *52*(D1), D672-D678. https://doi.org/10.1093/nar/gkad1025

Neisch, A. L., Neufeld, T. P., & Hays, T. S. (2017). A STRIPAK complex mediates axonal transport of autophagosomes and dense core vesicles through PP2A regulation. *J Cell Biol*, *216*(2), 441-461. https://doi.org/10.1083/jcb.201606082

Norris, F. A., Wilson, M. P., Wallis, T. S., Galyov, E. E., & Majerus, P. W. (1998). SopB, a protein required for virulence of Salmonella dublin, is an inositol phosphate phosphatase. *Proc Natl Acad Sci U S A*, *95*(24), 14057-14059. https://doi.org/10.1073/pnas.95.24.14057

Patel, J. C., Hueffer, K., Lam, T. T., & Galan, J. E. (2009). Diversification of a Salmonella virulence protein function by ubiquitin-dependent differential localization. *Cell*, *137*(2), 283-294. https://doi.org/10.1016/j.cell.2009.01.056

Perez-Riverol, Y., Bandla, C., Kundu, D. J., Kamatchinathan, S., Bai, J., Hewapathirana, S., John, N. S., Prakash, A., Walzer, M., Wang, S., & Vizcaino, J. A. (2025). The PRIDE database at 20 years: 2025 update. *Nucleic Acids Res*, *53*(D1), D543-D553. https://doi.org/10.1093/nar/gkae1011

Piscatelli, H. L., Li, M., & Zhou, D. (2016). Dual 4- and 5-phosphatase activities regulate SopB-dependent phosphoinositide dynamics to promote bacterial entry. *Cell Microbiol*, *18*(5), 705-719. https://doi.org/10.1111/cmi.12542

Prager, R., Mirold, S., Tietze, E., Strutz, U., Knuppel, B., Rabsch, W., Hardt, W. D., & Tschape, H. (2000). Prevalence and polymorphism of genes encoding translocated effector proteins among clinical isolates of Salmonella enterica. *Int J Med Microbiol*, *290*(7), 605-617. https://doi.org/10.1016/S1438-4221(00)80009-0

Ravikumar, B., Vacher, C., Berger, Z., Davies, J. E., Luo, S., Oroz, L. G., Scaravilli, F., Easton, D. F., Duden, R., O'Kane, C. J., & Rubinsztein, D. C. (2004). Inhibition of mTOR induces autophagy and reduces toxicity of polyglutamine expansions in fly and mouse models of Huntington disease. *Nat Genet*, *36*(6), 585-595. https://doi.org/10.1038/ng1362

Rescher, U., Ruhe, D., Ludwig, C., Zobiack, N., & Gerke, V. (2004). Annexin 2 is a phosphatidylinositol (4,5)-bisphosphate binding protein recruited to actin assembly sites at cellular membranes. *J Cell Sci*, *117*(Pt 16), 3473-3480. https://doi.org/10.1242/jcs.01208

Rodriguez-Escudero, I., Ferrer, N. L., Rotger, R., Cid, V. J., & Molina, M. (2011). Interaction of the Salmonella Typhimurium effector protein SopB with host cell Cdc42 is involved in intracellular replication. *Mol Microbiol*, *80*(5), 1220-1240. https://doi.org/10.1111/j.1365-2958.2011.07639.x

Rodriguez-Escudero, I., Rotger, R., Cid, V. J., & Molina, M. (2006). Inhibition of Cdc42-dependent signalling in Saccharomyces cerevisiae by phosphatase-dead SigD/SopB from Salmonella typhimurium. *Microbiology (Reading)*, *152*(Pt 11), 3437-3452. https://doi.org/10.1099/mic.0.29186-0

Rogers, L. D., Kristensen, A. R., Boyle, E. C., Robinson, D. P., Ly, R. T., Finlay, B. B., & Foster, L. J. (2008). Identification of cognate host targets and specific ubiquitylation sites on the Salmonella SPI-1 effector SopB/SigD. *J Proteomics*, *71*(1), 97-108. https://doi.org/10.1016/j.jprot.2008.01.011

Roppenser, B., Kwon, H., Canadien, V., Xu, R., Devreotes, P. N., Grinstein, S., & Brumell, J. H. (2013). Multiple host kinases contribute to Akt activation during Salmonella infection. *PLoS One*, *8*(8), e71015. https://doi.org/10.1371/journal.pone.0071015

Ruan, H., Zhang, Z., Tian, L., Wang, S., Hu, S., & Qiao, J. J. (2016). The Salmonella effector SopB prevents ROS-induced apoptosis of epithelial cells by retarding TRAF6 recruitment to mitochondria. *Biochem Biophys Res Commun*, *478*(2), 618-623. https://doi.org/10.1016/j.bbrc.2016.07.116

Schmid, E. W., & Walter, J. C. (2025). Predictomes, a classifier-curated database of AlphaFold-modeled protein-protein interactions. *Mol Cell*, *85*(6), 1216-1232 e1215. https://doi.org/10.1016/j.molcel.2025.01.034

Schwarz, N., Leube, R. E., & Dusterhoft, S. (2025). Comprehensive in silico analyses of keratin heterodimerisation. *Eur J Cell Biol*, *104*(4), 151513. https://doi.org/10.1016/j.ejcb.2025.151513

Shouib, R., & Eitzen, G. (2022). Cdc42 regulates cytokine expression and trafficking in bronchial epithelial cells. *Front Immunol*, *13*, 1069499. https://doi.org/10.3389/fimmu.2022.1069499

Steele-Mortimer, O., Knodler, L. A., Marcus, S. L., Scheid, M. P., Goh, B., Pfeifer, C. G., Duronio, V., & Finlay, B. B. (2000). Activation of Akt/protein kinase B in epithelial cells by the Salmonella typhimurium effector sigD. *J Biol Chem*, *275*(48), 37718-37724. https://doi.org/10.1074/jbc.M008187200

Steinegger, M., & Soding, J. (2017). MMseqs2 enables sensitive protein sequence searching for the analysis of massive data sets. *Nat Biotechnol*, *35*(11), 1026-1028. https://doi.org/10.1038/nbt.3988

Terebiznik, M. R., Vieira, O. V., Marcus, S. L., Slade, A., Yip, C. M., Trimble, W. S., Meyer, T., Finlay, B. B., & Grinstein, S. (2002). Elimination of host cell PtdIns(4,5)P(2) by bacterial SigD promotes membrane fission during invasion by Salmonella. *Nat Cell Biol*, *4*(10), 766-773. https://doi.org/10.1038/ncb854

Truong, D., Boddy, K. C., Canadien, V., Brabant, D., Fairn, G. D., D'Costa, V. M., Coyaud, E., Raught, B., Perez-Sala, D., Park, W. S., Heo, W. D., Grinstein, S., & Brumell, J. H. (2018). Salmonella exploits host Rho GTPase signalling pathways through the phosphatase activity of SopB. *Cell Microbiol*, *20*(10), e12938. https://doi.org/10.1111/cmi.12938

Turei, D., Korcsmaros, T., & Saez-Rodriguez, J. (2016). OmniPath: guidelines and gateway for literature-curated signaling pathway resources. *Nat Methods*, *13*(12), 966-967. https://doi.org/10.1038/nmeth.4077

UniProt, C. (2025). UniProt: the Universal Protein Knowledgebase in 2025. *Nucleic Acids Res*, *53*(D1), D609-D617. https://doi.org/10.1093/nar/gkae1010

Varga, J. K., Ovchinnikov, S., & Schueler-Furman, O. (2025). actifpTM: a refined confidence metric of AlphaFold2 predictions involving flexible regions. *Bioinformatics*, *41*(3). https://doi.org/10.1093/bioinformatics/btaf107

Walpole, G. F. W., Pacheco, J., Chauhan, N., Clark, J., Anderson, K. E., Abbas, Y. M., Brabant-Kirwan, D., Montano-Rendon, F., Liu, Z., Zhu, H., Brumell, J. H., Deiters, A., Stephens, L. R., Hawkins, P. T., Hammond, G. R. V., Grinstein, S., & Fairn, G. D. (2022). Kinase-independent synthesis of 3-phosphorylated phosphoinositides by a phosphotransferase. *Nat Cell Biol*, *24*(5), 708-722. https://doi.org/10.1038/s41556-022-00895-y

Wang, Z., Karkossa, I., Grosskopf, H., Rolle-Kampczyk, U., Hackermuller, J., von Bergen, M., & Schubert, K. (2021). Comparison of quantitation methods in proteomics to define relevant toxicological information on AhR activation of HepG2 cells by BaP. *Toxicology*, *448*, 152652. https://doi.org/10.1016/j.tox.2020.152652

Weigert, A., & Herhaus, L. (2024). Immune modulation through secretory autophagy. *J Cell Biochem*, *125*(11), e30427. https://doi.org/10.1002/jcb.30427

Xu, P., Liu, J., Sakaki-Yumoto, M., & Derynck, R. (2012). TACE activation by MAPK-mediated regulation of cell surface dimerization and TIMP3 association. *Sci Signal*, *5*(222), ra34. https://doi.org/10.1126/scisignal.2002689

Zhang, K., Dupont, A., Torow, N., Gohde, F., Leschner, S., Lienenklaus, S., Weiss, S., Brinkmann, M. M., Kuhnel, M., Hensel, M., Fulde, M., & Hornef, M. W. (2014). Age-dependent enterocyte invasion and microcolony formation by Salmonella. *PLoS Pathog*, *10*(9), e1004385. https://doi.org/10.1371/journal.ppat.1004385

Zhang, K., Repnik, U., Diab, N., Friske, D., Putz, A., Bachmann, A. Z., Gubbi, N., Hensel, M., Forstner, K. U., Westermann, A. J., Dupont, A., & Hornef, M. W. (2024). Non-

professional efferocytosis of Salmonella-infected intestinal epithelial cells in the neonatal host. *J Exp Med*, *221*(3). https://doi.org/10.1084/jem.20231237

Zhang, K., Riba, A., Nietschke, M., Torow, N., Repnik, U., Putz, A., Fulde, M., Dupont, A., Hensel, M., & Hornef, M. (2018). Minimal SPI1-T3SS effector requirement for Salmonella enterocyte invasion and intracellular proliferation in vivo. *PLoS Pathog*, *14*(3), e1006925. https://doi.org/10.1371/journal.ppat.1006925

Zhao, S., Xu, Q., Cui, Y., Yao, S., Jin, S., Zhang, Q., Wen, Z., Ruan, H., Liang, X., Chao, Y., Gong, S., Sansonetti, P., Wei, K., Tang, H., & Jiu, Y. (2023). Salmonella effector SopB reorganizes cytoskeletal vimentin to maintain replication vacuoles for efficient infection. *Nat Commun*, *14*(1), 478. https://doi.org/10.1038/s41467-023-36123-w

Zhou, D., Chen, L. M., Hernandez, L., Shears, S. B., & Galan, J. E. (2001). A Salmonella inositol polyphosphatase acts in conjunction with other bacterial effectors to promote host cell actin cytoskeleton rearrangements and bacterial internalization. *Mol Microbiol*, *39*(2), 248-259. https://doi.org/10.1046/j.1365-2958.2001.02230.x

Figure legends

Figure 1. Host survival and infection-induced chemokine and cytokine expression. (a) Kaplan-Meier curve of 1-day-old C57BL/6 wildtype mice orally infected with 100 CFU wt (n=7), *sopB*-deficient (Δ*sopB*, n=7), or *sopB*-deficient *S.* Typhimurium complemented in trans with *sopB* and its chaperon *sigE* (Δ*sopB* p*sopB sigE*, compl., n=7). **(b-e)** 1-day-old mice were left non-infected (n=3-4) or orally infected with wt (n=4-10), *sopB*-deficient (Δ*sopB*, n=4-14), *sopB*-deficient *S.* Typhimurium complemented in trans with *sopB* and its chaperon *sigE* (Δ*sopB* p*sopBsigE*, compl., n=4-9) or $sopE_2$ deficient *S.* Typhimurium (Δ$sopE_2$, n=7-8). Number of intracellular *S.* Typhimurium in isolated intestinal epithelial cells at day 1 **(b)** and 2 **(c)** post infection **(**p.i.). One data point represents one animal, at least two independent experiments. Mean. *Cxcl1*, *Cxcl2* and *Ccl2* mRNA expression in total isolated intestinal epithelial cells at day 1 **(d)** and day 2 **(e)** p.i. Values were normalised to the house keeping gene *Hprt* and are showed as fold expression over uninfected age-matched control animals. One data point represents one animal from at least two independent experiments, median. **(f)** Color-scaled heat map (z-score) showing the concentration of the indicated cytokines and chemokines in sera of uninfected age-matched animals (n=3), or mice infected at day 1 after birth with wt (n=3) or Δ*sopB S.* Typhimurium (n=3-4) at day 1 and 2 p.i. Each column represents one animal. Statistical analysis by log-rank (Mantel-Cox) test (**A**), Kruskal-Wallis test combined with Dunn's multiple comparison test (**b-e**); two-way ANOVA with Sidak's multiple comparison test (**f**). *, $p<0.05$; **, $p<0.01$, ***, $p<0.001$.

Figure 2. Immune cell infiltration in mucosal tissue. (a-c) 1-day-old C57BL/6 wildtype neonates were orally infected with 100 CFU wt (n=3 at day 1 and 2 p.i.) or *sopB*-deficient (Δ*sopB*, n=3 and n=4 at day 1 and 2 p.i., respectively) *S.* Typhimurium. Flow cytometric analysis of *lamina propria* $Ly6C^{hi}Ly6G^{-}CD11b^{+}$ $MHCII^{lo/-}CD45^{+}DAPI^{-}$ monocytes **(a),** $Ly6G^{+}Ly6C^{int}CD11b^{+}$ $MHCII^{lo/-}CD45^{+}DAPI^{-}$ neutrophils **(b)** and $CD64^{+}MHCII^{+}CD45^{+}DAPI^{-}$ macrophages **(c). (d-f)** Immunostaining **(d)** of small intestine tissue sections of age-matched uninfected animals and neonate mice infected with wt or *sopB*-deficient (Δ*sopB*) *S.* Typhimurium at day 1 and 2 p.i. for $Ly6G^{+}$ neutrophils (PMN, red). WGA (white), and DAPI (blue). Bar=50 µm, white boxes indicate the position of the enlarged images, insert i and ii, 20 µm. Representative images are shown. **(e and f)** Quantification of the number of $Ly6G^{+}$ neutrophils (PMNs) per mm^2 of small intestinal tissue at day 1 p.i. analysing a total area of 0.38 mm^2, and at day 2 p.i. analysing a total area of 0.10 mm^2. Uninfected, age-matched neonates (4

or 8-11 images per animal at day 1 or 2 p.i., respectively, both n=3) or neonates infected with wt (4 or 4-12 images per animal at day 1 or 2 p.i., respectively, both n=3) or Δ*sopB S.* Typhimurium (4 or 5-17 images per animal at day 1 or 2 p.i., respectively, both n=3). Statistical analysis by two-way ANOVA with Tukey's multiple comparison test (**a-c**) and Kruskal-Wallis combined with Dunn's multiple comparison test (**e and f**). ns, non-significant; *, p<0.05; **, p<0.01; ****, p<0.0001.

Figure 3. Histological characterisation of the neonatal small intestine following infection. **(a)** H&E stained tissue sections of non-infected, wt or Δ*sopB S.* Typhimurium infected neonates at day 2 p.i. Bar=100 µm. **(b)** *Lamina propria* depth in 15-20 areas per non-infected (n=3), wt (n=3), or Δ*sopB*-infected (n=3) animal. **(c)** MUC2 immunostaining (red) in tissue sections of non-infected (n=3), wt (n=3), or Δ*sopB S.* Typhimurium-infected (n=3) animals at day 2 p.i. Counterstaining with WGA (white), DAPI (blue); autofluorescence (green). Bar=50 µm. **(d)** Percentage of goblet cells among intestinal epithelial cells in non-infected (n=3), wt (n=3), or Δ*sopB* (n=3) *S.* Typhimurium-infected animals at day 2 p.i. 10-20 images with the size of 312µm x 250µm were evaluated per animal. **(e)** $MUC2^+$ goblet cell size in tissue sections of uninfected (n=3), wt (n=3) or Δ*sopB* (n=3) *S.* Typhimurium-infected animals at day 2 p.i. 11-21 goblet cells (μm^2) were analysed on each section. **(f)** TUNEL staining (red) of tissue sections of non-infected (n=2), wt (n=5), or Δ*sopB* (n=4) *S.* Typhimurium-infected animals at day 2 p.i. White boxes indicate enlarged images (i, ii). Counterstaining with DAPI (blue). Bar=50 µm; insert, 20 µm. **(g)** Number of $TUNEL^+$ cells in tissue sections of uninfected (n=2), wt (n=5), or Δ*sopB* (n=4) *S.* Typhimurium-infected animals at day 2 p.i. 9 -12 images with the size of 624µm x 501µm were evaluated per animal. **(h)** Ki67 (red) immunostaining on tissue sections of neonates infected with wt (n=3) or Δ*sopB* (n=4) *S.* Typhimurium at day 2 p.i. Counterstaining with E-cadherin (green), WGA (white), and DAPI (blue). Bar, 50 µm, insert, 20 µm. **(i)** Number of $Ki67^+$ cells in tissue sections of uninfected (n=2), wt (n=5), or Δ*sopB* (n=4) *S.* Typhimurium-infected animals at day 2 p.i. 5-29 intervillus junctions (early crypts) were analysed per section. Representative images are shown. Quantified data are shown as individual points in violin plots, solid lines represent the median. Statistical analysis by Kruskal-Wallis combined with Dunn's multiple comparison test (**b, d, and g**), one-way ANOVA with Tukey's multiple comparison test (**e**) and Mann-Whitney test **(i)**. ns, non-significant; *, p<0.05; ****, p<0.0001.

Figure 4. Mechanisms of disease progression at day 2 p.i. (a-c) Kaplan-Meier curve of wildtype (n=7 both groups) and *Casp1*$^{-/-}$ (n=8-9) **(a)**, wildtype and intestinal epithelium-specific

caspase 8-deficient (*Casp8*$^{\Delta IEC}$, n=12) **(b)**, and wildtype and *Mlkl*$^{-/-}$ (n=16) **(c)** neonates infected with wt or Δ*sopB S.* Typhimurium. **(d)** H&E staining of tissue sections of wildtype (n=3) and *Mlkl*$^{-/-}$ (n=3) Δ*sopB S.* Typhimurium infected neonates at day 2 p.i. Bar=50 µm. **(e)** Depth of the *lamina propria* in 4-12 areas per wildtype or *Mlkl*$^{-/-}$ mouse infected with wt or Δ*sopB S.* Typhimurium at day 2 p.i. Individual data points and median. **(f)** H&E staining of tissue sections from neonatal wildtype (n=3) and *Tnfrsf1a*$^{-/-}$ (n=5) mice infected with Δ*sopB S.* Typhimurium at day 2 p.i. Bar=50 µm. **(g)** Fold change of the depth of the *lamina propria* in Δ*sopB S.* Typhimurium-infected over non-infected age-matched wildtype (n=3 and 3) and *Tnfrsf1a*$^{-/-}$ mice (n=3 and 3) at day 2 p.i. 3-9 fields were analysed per animal. Individual data points and median. **(h)** Kaplan-Meier curve of wildtype (n=7) and *Tnfrsf1a*$^{-/-}$ (n=9-12) neonates infected with wt or Δ*sopB S.* Typhimurium. **(i)** *Tnf* mRNA in total gut tissue from age-matched non-infected (n=3), wt (n=7), or Δ*sopB* (n=3) *S.* Typhimurium-infected animals at day 2 p.i. Fold increase, values are normalised to *Hprt*. At least two independent experiments. One data point represents one animal, Median. **(j)** Viability of unstimulated (left panel) or PMA/ionomycin stimulated (right panel) *lamina propria* monocytes of wt (black circles, n=4) or Δ*sopB* (red squares, n=4) *S.* Typhimurium infected animals. Mean ± SD. **(k)** TNFα mean fluorescence intensity (MFI) after intracellular cytokine staining at day 2 p.i. from wt (n=4) or Δ*sopB* (n=4) *S.* Typhimurium-infected animals without (left panel) or after stimulation with PMA/ionomycin (right panel). Median. (**a-c and h**) The groups of infected wildtype mice are identical to Figure 1a. Log-rank (Mantel-Cox) test (**a-c and h**), Kruskal–Wallis test with Dunn's multiple comparisons post-test (**e**), one-way ANOVA with Tukey's multiple comparison test (**i**), Mann-Whitney test **(g and j**), and two-way ANOVA with Sidak's multiple comparison test (**k**). ns, non-significant; *, p<0.05; **, p<0.01; ***, p<0.001; ****, p<0.0001.

Figure 5. Influence of SopB on ADAM17 activation and TNF secretion at day 1 p.i. (a and b) Comparative intestinal epithelial *Cxcl2* mRNA expression in non-infected wt or Δ*sopB S.* Typhimurium-infected wildtype **(a)** and *Tnfrsf1a*$^{-/-}$ **(b)** mice. Wildtype, n=4, 10, 14 (identical to Fig. 1d) and *Tnfrsf1a*$^{-/-}$, n=6, 7, 6 animals, respectively. Values normalised to *Hprt*; fold expression over non-infected animals. At least two independent experiments, median. **(c)** Gene set enrichment analysis (GSEA) using bulk RNA Seq data from intestinal epithelial cells isolated at day 1 p.i. from wt (n=4) and Δ*sopB* (n=4) *S.* Typhimurium-infected wildtype neonates (see Suppl. Fig. 1g). **(d-g)** *Tnf* mRNA expression in intestinal epithelial cells **(d)**, CD64^{+}MHCII^{+}CD45^{+}DAPI^{-} macrophages **(e)**, Ly6C^{hi}Ly6G^{-}CD11b^{+} MHCII$^{lo/-}$CD45^{+}DAPI^{-} monocytes **(f)**, and Ly6G^{+}Ly6C^{int}CD11b^{+} MHCII$^{lo/-}$CD45^{+}DAPI^{-} neutrophils **(g)** isolated from

non-infected (n=3), wt (n=7), or Δ*sopB* (n=10) *S.* Typhimurium-infected mice at day 1 p.i. **(d)** or sorted by flow cytometry from non-infected (n=3), wt (n=3), or Δ*sopB* (n=3) *S.* Typhimurium-infected neonates at day 1 p.i. **(e-g)**. Values normalised to *Hprt*; median. **(h)** Intestinal epithelial cells from neonates isolated at day 1 p.i. with wt (n=~~3~~) or Δ*sopB S.* Typhimurium (n=3) incubated with ADAM17 substrate in the presence or absence of a specific ADAM17 inhibitor. Enzymatic activity was quantified at Ex/Em=320 nm/420 nm. **(i)** ADAM17^{+} surface relative to the total apical epithelial surface measured using the ZEN 3.4 imaging software [%]. 86-88 villi per tissue from wt (n=2), Δ*sopB S.* Typhimurium (n=5) infected and non-infected animals (n=2). **(j)** ADAM17 immunostaining (red) in non-infected, wt or Δ*sopB S.* Typhimurium-infected neonates. Counterstaining: EpCam (green), wheat germ agglutinin (WGA, white) and DAPI. Bar=25 µm. **(k)** TNFα (MFI) in the supernatant of cultured (2 h) segments of intestine from non-infected (n=3), wt (n=7), or Δ*sopB* (n=9) *S.* Typhimurium-infected neonates. Normalised to non-infected animals. Mean ± SD of two independent experiments. **(l)** *Tnfrsf1a* mRNA expression in intestinal epithelial cells isolated at day 1 p.i. with wt or Δ*sopB S.* Typhimurium (wt, n=4; Δ*sopB*, n=4). Values from the RNA Seq dataset in Suppl. Fig. 1g. Fold change over the mean of non-infected animals (n=4). Median. Statistical analysis by Kruskal-Wallis combined with Dunn's multiple comparison test (**a, b, e, g, i**), one-way ANOVA with Tukey's multiple comparison test (**d, k, f**), and student's t-test (**l**). ns, non-significant; *, p<0.05; **, p<0.01; ***, p<0.001; ****, p<0.0001.

Fig. 6: Analysis of the interaction of SopB with host cell processes (a) Phosphoproteome of m-IC$_{cl2}$ cells left untreated (n=4) or infected with wt (n=4), Δ*sopB* (n=4) or Δ*sopB* p*sopBsigE* *S.* Typhimurium (compl., n=4) for 1 h. Qiagen Ingenuity Pathway Analysis based on significantly altered phosphosites using the IPA Z-score activation scaling. Adjusted P-values (Benjamini-Hochberg correction) indicate differences from non-infected cells. **(b)** Top ten GO terms based on genes significantly upregulated in wt (n=4) relative to Δ*sopB* (n=4) *S.* Typhimurium-infected neonates at day 1 p.i. **(c)** Affinity purification and mass spectrometric analysis of SopB-associated host cell proteins. m-IC$_{cl2}$ cells were infected for 1 h with wt or *S.* Typhimurium carrying a triple FLAG-conjugated SopB. X-axis, $\log_2$ fold changes ($\log_2$FC) relative to control; y-axis, -$\log_{10}$(p-value) for differential abundance. Dashed lines indicate thresholds for differential enrichment ($|\log_2 FC| \geq 0.33$) and nominal significance ($p < 0.05$). SopB-FLAG pull-down enriched proteins in red. No proteins passed the threshold for multiple testing (adjusted p-value). **(d and e)** Interaction-confidence landscape and connectivity between the SopB interactome identified in **(c)** and the ADAM17 protein complex. **(d)** Heatmap of

AlphaFold-Multimer–derived interaction confidence for selected pairwise combinations (all tested combinations in Suppl. Fig. 6b). **(e)** Integrated network connecting SopB interactome and ADAM17 complex using AFM-augmented PPIs (interaction confidence > 0.75) and curated kinase-substrate links from databases. Filtered to retain only direct links or connections via a single intermediate node. **(f-g)** IL-18 **(f)** and IL-6 **(g)** concentration (MFI over non-infected control) in supernatants of stem cell organoid cultures infected with wt or Δ*sopB S.* Typhimurium in the presence or absence of rapamycin measured by cytometric bead array. Mean ± SD of four independent experiments. **(h)** IL-18 (MFI over non-infected control) in the supernatant of longitudinally opened intestinal tissue segments from non-infected (n=3), wt (n=7), or Δ*sopB* (n=9) *S.* Typhimurium-infected neonates cultured *ex vivo* for 2 h. Cytokine bead array. Mean ± SD from two independent experiments. Statistical analysis by Kruskal-Wallis combined with Dunn's multiple comparison test (**f and g**) and one-way ANOVA Kruskal–Wallis test with Dunn's post-test (**h**). ns, non-significant; *, $p<0.05$; **, $p<0.01$; ***, $p<0.001$.

Figure 7. Functional influence of the C- and N-terminal domain on the immune-suppressive phenotype of SopB. (a-c) Kaplan-Meier curve of 1-day-old C57BL/6 wildtype mice orally infected with 100 CFU wt (n=7), *sopB* deficient (Δ*sopB*, n=7) *S.* Typhimurium, or S. Typhimurium strains carrying a point mutation in the C-terminal domain of SopB (*sopB*^{C460S}, n=5, **(a)**; and *sopB*^{K528A}, n=4, **(b)**) or N-terminal domain of SopB (*sopB*^{L76P}, n=15, **(c)**). Note that the groups of wt and Δ*sopB S.* Typhimurium-infected wildtype mice are identical to Figure 1A. log-rank (Mantel-Cox) test. **(d-f)** *Cxcl1* **(d)**, *Ccl2* **(e)** and *Cxcl2* **(f)** expression in total isolated intestinal epithelial cells isolated at day 1 p.i. from age-matched non-infected mice or mice orally infected with wt (n=5-7), Δ*sopB* (n=7-14), Δ*sopB* p*sopBsigE* (compl., n=4-7) or chromosomally *sopB*^{L76P} carrying *S.* Typhimurium (n=9). Values were normalised to the house keeping gene *Hprt* and are showed as fold expression over uninfected age-matched control animals (n=3-4). One data point represents one animal from at least two independent experiments, median. (**g and h**) Flow cytometric analysis of *lamina propria* Ly6C^{hi}Ly6G^{-} CD11b^{+} MHCII$^{lo/-}$CD45^{+}DAPI^{-} monocytes and Ly6G^{+}Ly6C^{int}CD11b^{+} MHCII$^{lo/-}$CD45^{+}DAPI^{-} neutrophils in 1-day-old C57BL/6 wildtype neonates orally infected with 100 CFU wt (n=3 at day 1 and 2 p.i.), *sopB* deficient (Δ*sopB*, n=3 and n=4 at day 1 and 2 p.i., respectively) or *sopB*^{L76P} carrying *S.* Typhimurium (n=7 and n=4 at day 1 and 2 p.i., respectively). (**g and h**) The groups of wt and Δ*sopB*-infected mice are identical to Fig. 2a and b. Statistical analysis by

Kruskal-Wallis combined with Dunn's multiple comparison test (**d-f**) and two-way ANOVA with Tukey's multiple comparison test (**g and h**). ns, non-significant; *, $p<0.05$; **, $p<0.01$.

Supplemental figure legends

Suppl. Figure 1. (a) Schematic diagram of the neonatal small intestinal epithelial stem cell organoid co-culture. Stem cell organoid cells grown as monolayers were infected for 1 h with wt, Δ*sopB*, or Δ*sopB* p*sopBsigE* (compl.) *S.* Typhimruium followed by a 1h incubation in 100 µg/mL gentamicin at 37°C. The number of viable bacteria analysed by serial dilution and plating. **(b)** Invasion rate expressed as the number of detected intracellular bacteria relative to the number of administered bacteria x 100 (in %). One data point represents one infected well, mean ± SD, three independent experiments. **(c and d)** Total bacterial count in mesenteric lymph node (MLN), liver and spleen tissue at day 1 **(c)** and 2 **(d)** p.i. **(e and f)** *Reg3g* and *Cxcl5* mRNA expression in total isolated intestinal epithelial cells at day 1 **(e)** and 2 **(f)** p.i. 1-day-old mice were left untreated (n=3) or infected with wt (n=5-11), Δ*sopB* (n=4-14), Δ*sopB* p*sopBsigE* (compl., n=4-9), or Δ*sopE*$_2$ (n=7-8, only for *Cxcl5*) *S.* Typhimurium. Values normalised to *Hprt;* shown as fold expression over non-infected controls. One data point represents one animal from at least two independent experiments, median. **(g)** Volcano plot of genes significantly differentially expressed (p adjusted<0.05 and |log2FC|>1) by intestinal epithelial cells isolated from wt (n=4) *versus* Δ*sopB S.* Typhimurium-infected wildtype neonates (n=4) at d1 p.i.. Genes with increased expression in Δ*sopB S.* Typhimurium-infected mice are shown in red; genes with increased expression in wt *S.* Typhimurium-infected mice in blue. **(h)** Data from the color-scaled heat map (z-score) shown in Fig. 1f. Serum concentration of the indicated cytokines and chemokines in pg/mL in the serum of mice infected with wt (n=3, empty black circles) or Δ*sopB* (n=3-4, red circles) *S.* Typhimurium at day 1 and 2 p.i. Mean ± SD. One data point represents one animal. The dashed line indicates the detection limit of the assay. One-way ANOVA **(b)**, Kruskal-Wallis combined with Dunn's multiple comparison test (**c-f**); two-way ANOVA with Sidak's multiple comparison test (**h**). non-significant; *, p<0.05; **, p<0.01; ***, p<0.001; ****, p<0.0001.

Suppl. Figure 2. (a) Gating strategy to identify *lamina propria* $Ly6C^{hi}Ly6G^{-}CD11b^{+}$ $MHCII^{lo/-}$ $CD45^{+}DAPI^{-}$ monocytes, $Ly6G^{+}Ly6C^{int}CD11b^{+}$ $MHCII^{lo/-}CD45^{+}DAPI^{-}$ neutrophils and $CD64^{+}MHCII^{+}CD45^{+}DAPI^{-}$ macrophages by flow cytometric analysis (see Fig. 2).

Suppl. Figure 3. 9-week-old adult female mice were pretreated with streptomycin (20 mg) and 1 day later orally infected with wt (n=12) or Δ*sopB S.* Typhimurium (n=12) in PBS. Age-matched adult female mice treated with streptomycin and PBS were used as control (Co., n=14).

(a) Total body weight was monitored daily from one day prior to infection until 2 days p.i. **(b)** The bacterial load in liver, spleen, mesenteric lymph nodes (MLN) and colon and the intraepithelial CFU determined by dilution and plating. **(c-d)** *Cxcl2*, *Cxcl1 and Ccl2* mRNA expression in **(c)** total isolated intestinal epithelial cells and **(d)** colon tissue at day 2 p.i. (wt, n=4-8, Δ*sopB*, n=4-8**,** co., n=4-12**).** Values normalised to *Hprt* and are shown as fold expression over non-infected controls. **(e)** Representative image of small intestinal tissue sections stained with H&E of non-infected age-matched control animals or adult mice infected with wt or Δ*sopB S.* Typhimurium at day 2 p.i. Bar=100 µm. **(f)** Flow cytometric analysis of *lamina propria* $Ly6C^{hi}Ly6G^{-}CD11b^{+}MHCII^{lo/-}CD45^{+}DAPI^{-}$ monocytes, $Ly6G^{+}Ly6C^{int}CD11b^{+}MHCII^{lo/-}CD45^{+}DAPI^{-}$ neutrophils and $CD64^{+}MHCII^{+}CD45^{+}DAPI^{-}$ macrophages isolated at 2 days p.i. from wt (n=8) or Δ*sopB S.* Typhimurium (n=8) infected adult mice or healthy age-matched control animals (Co.). One data point represents one animal. 3 independent experiments, median. Kruskal-Wallis with Dunn's posttest (**b-f**). ns, non-significant.

Suppl. Figure 4. **(a)** Kaplan-Meier curve of 1-day-old wildtype (B6JWT, n=7 for both groups) and $Asc^{-/-}$ (n=6-14) neonates infected with wt or Δ*sopB S.* Typhimurium. Note that the groups of wt and Δ*sopB S.* Typhimurium-infected wildtype mice are identical to Figure 1a. **(b and c)** Quantitative RT-PCR analysis for *Bcl2* **(b)** and *Nos2* **(c)** mRNA expression in total intestinal epithelial cells isolated at day 2 p.i. from wildtype neonates infected at day 1 after birth with wt (n=6-7) or Δ*sopB* (n=6-9) *S.* Typhimurium or non-infected controls (n=3-5). Median. One data point represents one animal. **(d-f)** CFU of *sopB*-deficient (Δ*sopB*) *S.* Typhimurium in total isolated gentamicin-treated intestinal epithelial cells **(d)**, mesenteric lymph node (MLN) **(e)**, and liver tissue homogenates **(f)** of wildtype (n=3), $Mlkl^{-/-}$ (n=3), $Asc^{-/-}$ (n=4), $Casp1^{-/-}$ (n=5), and $Tnfrsf1a^{-/-}$ (n=7) mice at day 2 p.i. Median. One data point represents one animal. **(g)** Quantitative RT-PCR analysis for *Cxcl2* mRNA expression in total intestinal epithelial cells isolated at day 2 p.i. from wildtype (n=12), $Mlkl^{-/-}$ (n=3), $Asc^{-/-}$ (n=4), and $Casp1^{-/-}$ (n=5) neonates infected at day 1 after birth with Δ*sopB S.* Typhimurium. Kruskal Wallis test with Dunn's posttest (**b-g**). ns, non-significant; **, p<0.01; ***, p<0.001.

Suppl. Figure 5: (a) Gating strategy to identify *lamina propria* $Ly6C^{hi}Ly6G^{-}CD11b^{+}$ $MHCII^{lo/-}CD45^{+}DAPI^{-}$ monocytes, $Ly6G^{+}Ly6C^{int}CD11b^{+}$ $MHCII^{lo/-}CD45^{+}DAPI^{-}$ neutrophils and $CD64^{+}MHCII^{+}CD45^{+}DAPI^{-}$ macrophages by flow cytometric analysis. **(b and c)** Flow cytometric analysis of the viability of non-stimulated or PMA/ionomycin stimulated monocytes isolated from the *lamina propria* of wt (n=4) **(b)** or Δ*sopB* (n=4) **(c)** *S.* Typhimurium-infected

neonates at day 2 p.i. For this analysis, the upstream gating step on viable cells (see Fig. S4A) was omitted. **(d)** Flow cytometric staining of intracellular TNFα in $Ly6C^{hi}Ly6G^{-}CD11b^{+}$ $MHCII^{lo/-}CD45^{+}DAPI^{-}$ monocytes, $Ly6G^{+}Ly6C^{int}CD11b^{+}$ $MHCII^{lo/-}CD45^{+}DAPI^{-}$ neutrophils, and $CD64^{+}MHCII^{+}CD45^{+}DAPI^{-}$ macrophages isolated from wt (n=4) or Δ*sopB* (n=4) *S.* Typhimurium-infected mice at day 2 p.i. after re-stimulation with PMA/ionomycin.

Suppl. Figure 6: (a) Volcano plot of genes significantly differentially expressed (p adjusted<0.05 and |log2FC|>1) by intestinal epithelial cells isolated from wt (n=4) *versus* Δ*sopB S.* Typhimurium-infected *Tnfrsf1a*$^{-/-}$ neonates (n=4) at d1 p.i.. Genes with increased expression wildtype mice infected with Δ*sopB S.* Typhimurium (see Suppl. Fig. 1g) are shown in pink. **(b)** ADAM17 activity in intestinal epithelial cells isolated from mice infected with wt (n=3, left panel) or Δ*sopB S.* Typhimurium (n=3, right panel) and incubated with ADAM17 substrate for 30 min. in the presence (+ inhibitor) or absence of an ADAM17-specific inhibitor. For the full kinetic see Fig. 5h. One representative data set of three independent experiments. **(c)** Heatmap of AlphaFold-Multimer–derived interaction confidence for all pairwise combinations analysed between SopB interactome candidates (red, see Fig. 6c), ADAM17 complex proteins (black), and intermediate interacting molecules (grey, see Fig. 6e) deduced by generating an integrated network connecting SopB interactome and ADAM17 complex protein using AFM-augmented PPIs (interaction confidence > 0.75). **(d)** Western blot of material obtained by immunoprecipitation with an anti-FLAG antibody from wt and *sopB*::3xFLAG *S.* Typhimurium infected m-IC_{cl2} cells, as well as the bacterial pellet of *S.* Typhimurium *sopB*::3xFLAG (bacterial lysate) and total cell lysate of infected m-IC_{cl2} cells (cell lysate) using an anti-FLAG antibody (SopB) or an anti-ADAM17 antibody (ADAM17). M, prestained protein ladder. **(e)** CXCL2 secretion into the cell culture supernatant by m-IC_{cl2} cells left untreated (non-infected) or infected with wt or Δ*sopB S.* Typhimurium. One data point represents one technical replicate from at least two independent experiments, median ± SD. **(f)** Endotoxin in the basolateral compartment of m-IC_{cl2} cells grown on Transwell inserts and infected with wt or Δ*sopB S.* Typhimurium and the endotoxin (LPS) concentration was determined at 1, 2, and 3 h of co-culture using the Kinetic-QCL™ Kinetic Chromogenic LAL Assay (Lonza). Median ± SD. Paired t-test (**a**) and Kruskal-Wallis test with Dunn's posttest (**d and e**). ns, non-significant; **, p<0.01.

Suppl. Figure 7: (a and b) Total bacterial count in isolated total epithelial cells **(a)** and liver tissue **(b)** at day 2 p.i. with 100 CFU wt (n=4), *sopB* deficient (Δ*sopB*, n=3), *sopB* deficient in

trans *sopB* sigE complemented (Δ*sopB* p*sopBsigE*, n=3) or a *sopB*^{L76P} allele carrying *S.* Typhimurium (n=11-12). (**c**) Flow cytometric analysis of *lamina propria* CD64^{+}MHCII^{+}CD45^{+}DAPI^{-} macrophages in 1-day-old C57BL/6 wild-type neonates orally infected with 100 CFU wt (n=3 at day 1 and 2 p.i.), Δ*sopB* (n=3 and 4 at day 1 and 2 p.i., respectively) or *sopB*^{L76P}-expressing *S.* Typhimurium (*sopB*^{L76P}, n=7 and n=4 at day 1 and 2 p.i., respectively) at day 1 and 2 p.i. Kruskal-Wallis combined with Dunn's multiple comparison test (**a and b**) and two-way ANOVA with Tukey's multiple comparison test (**c**). ns, non-significant; *, $p<0.05$.

Diab et al., Figure 1

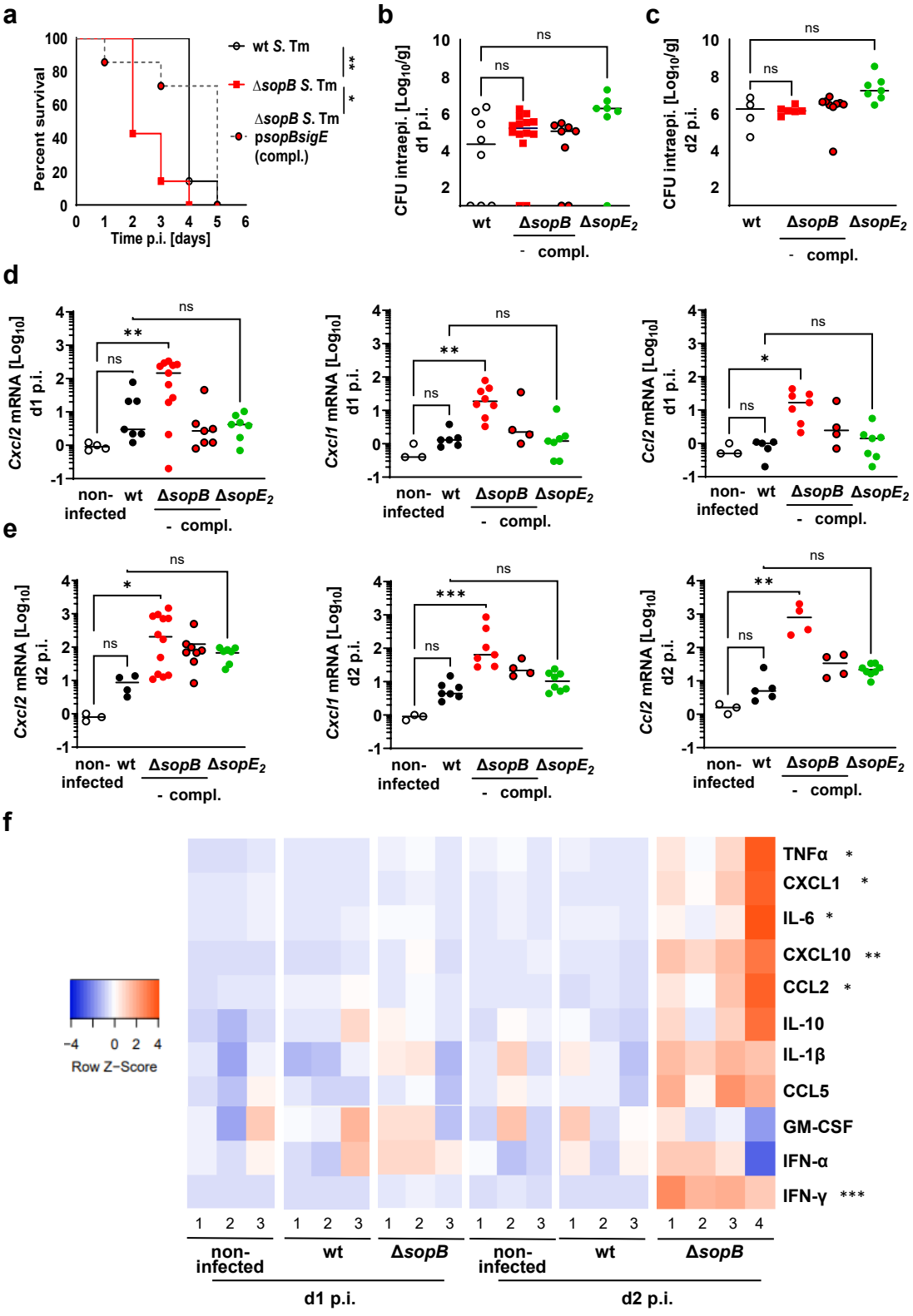

Diab et al., Figure 2

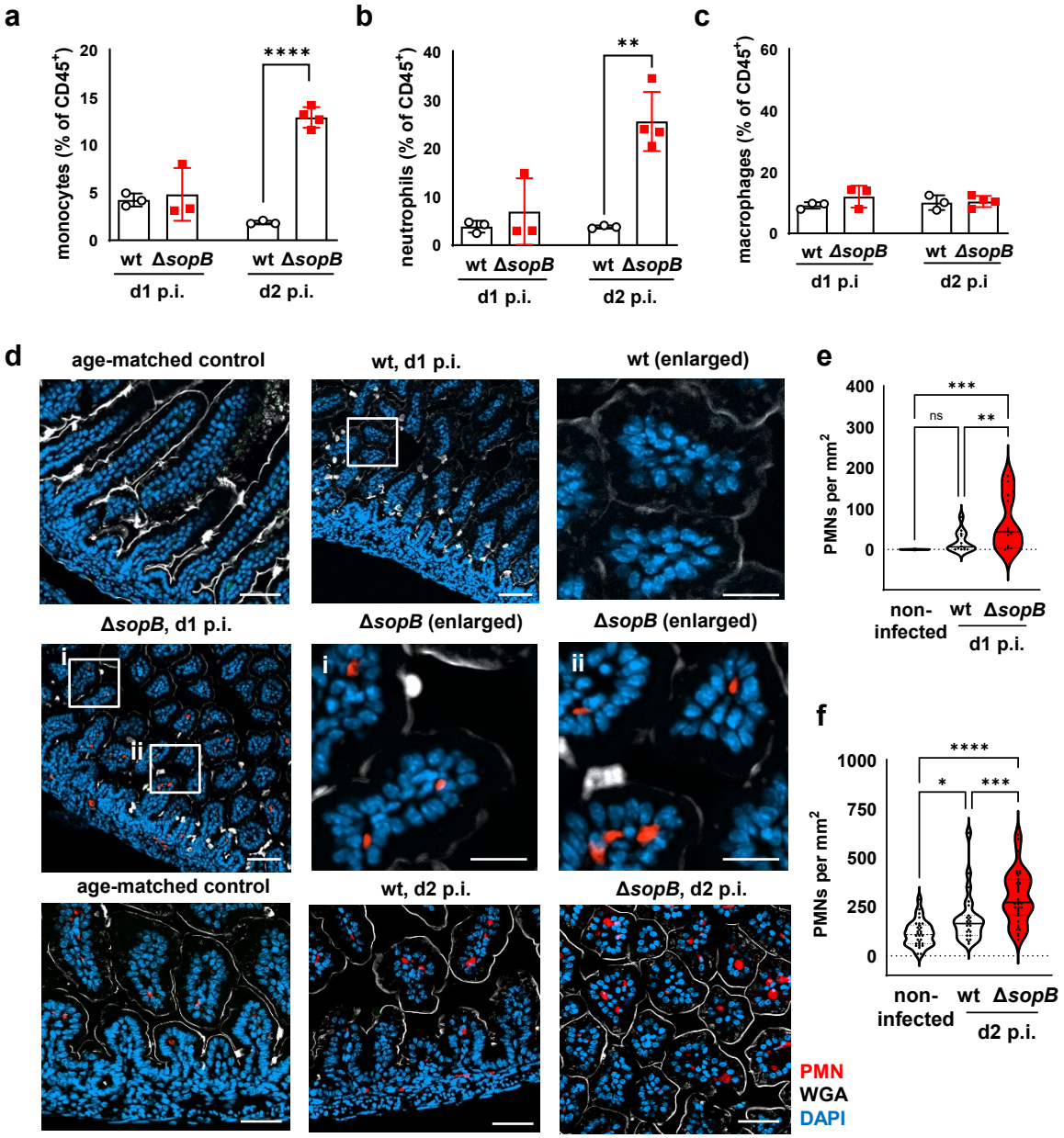

Diab et al., Figure 3

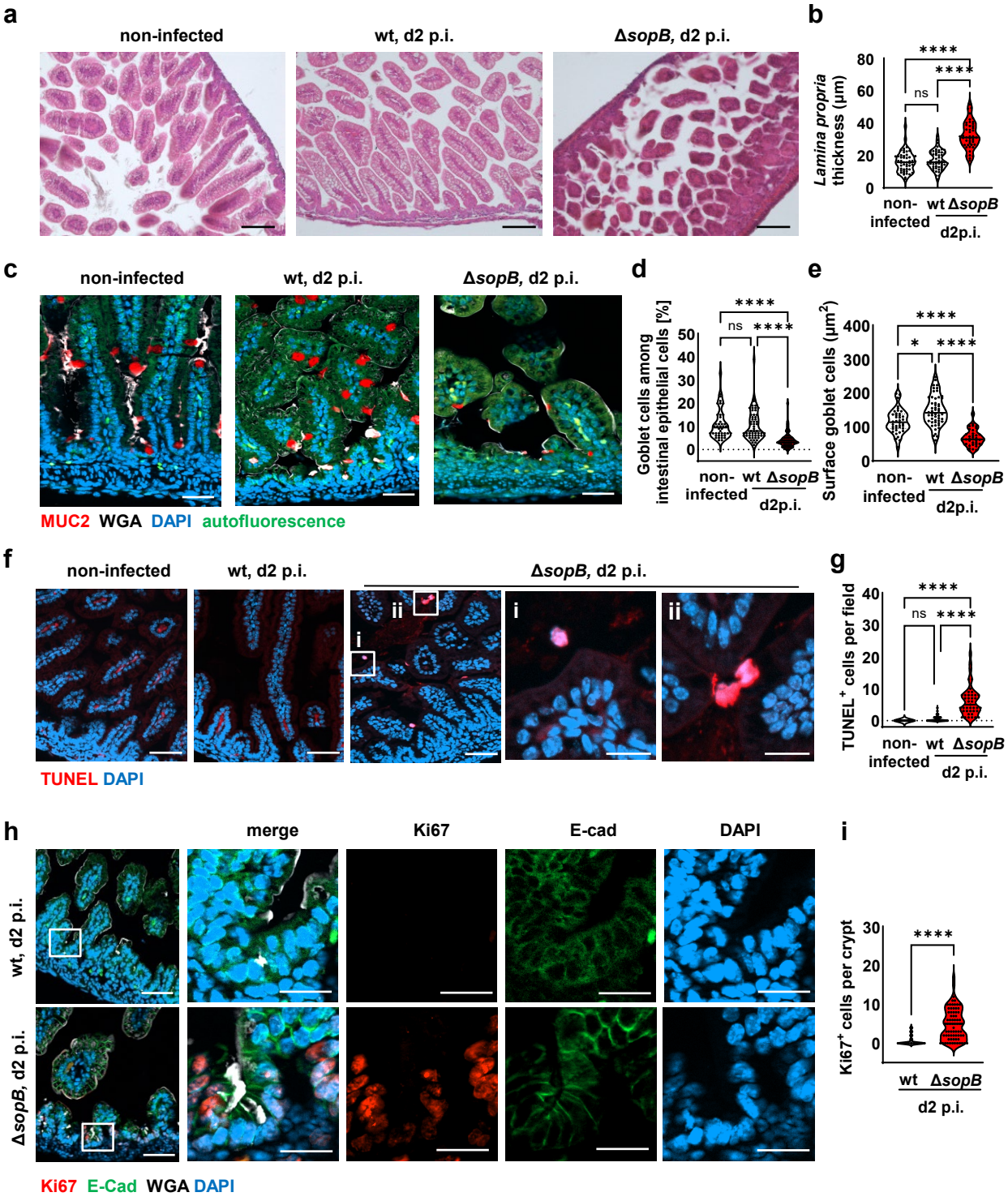

Diab et al., Figure 4

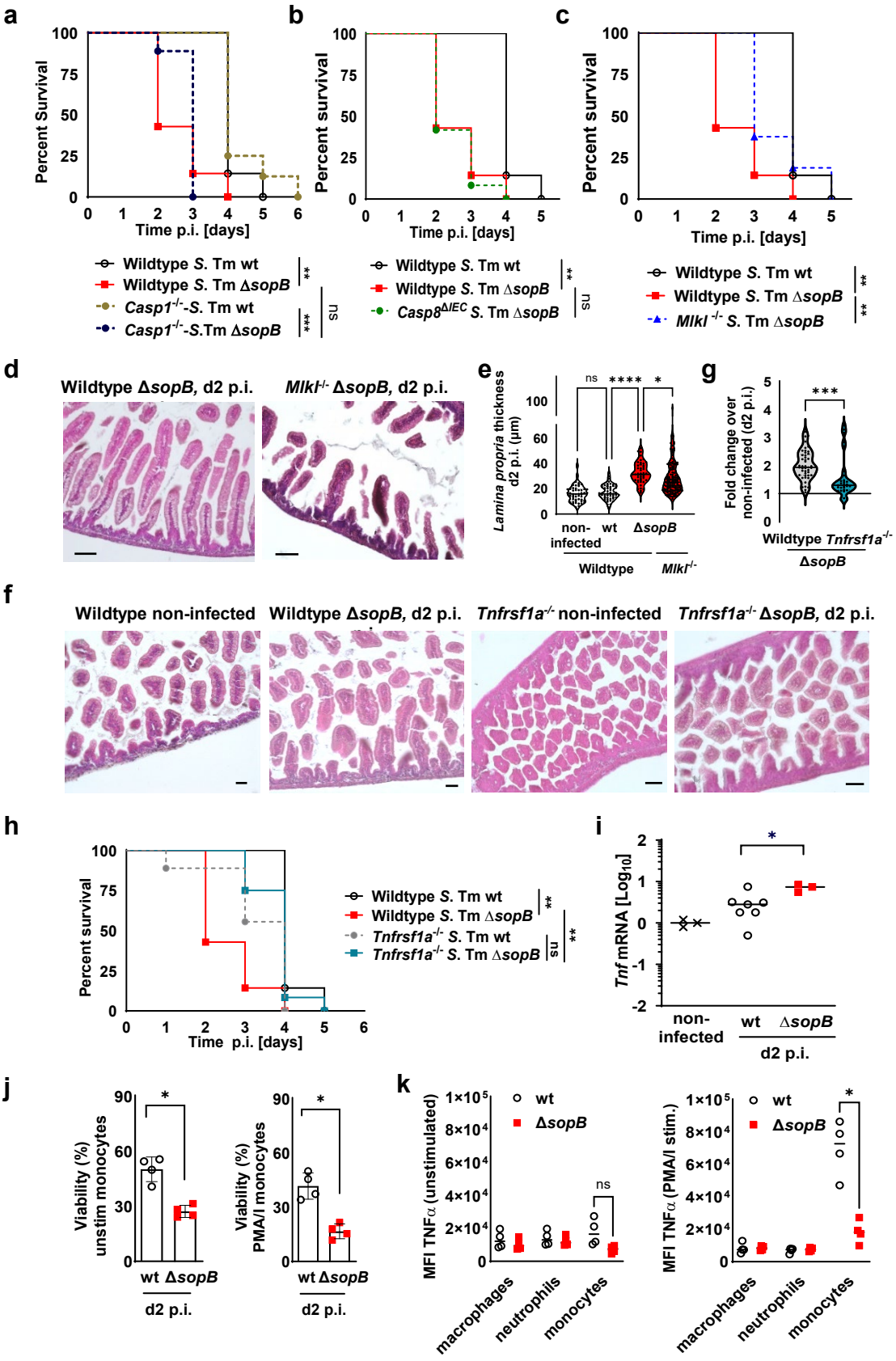

Diab et al., Figure 5

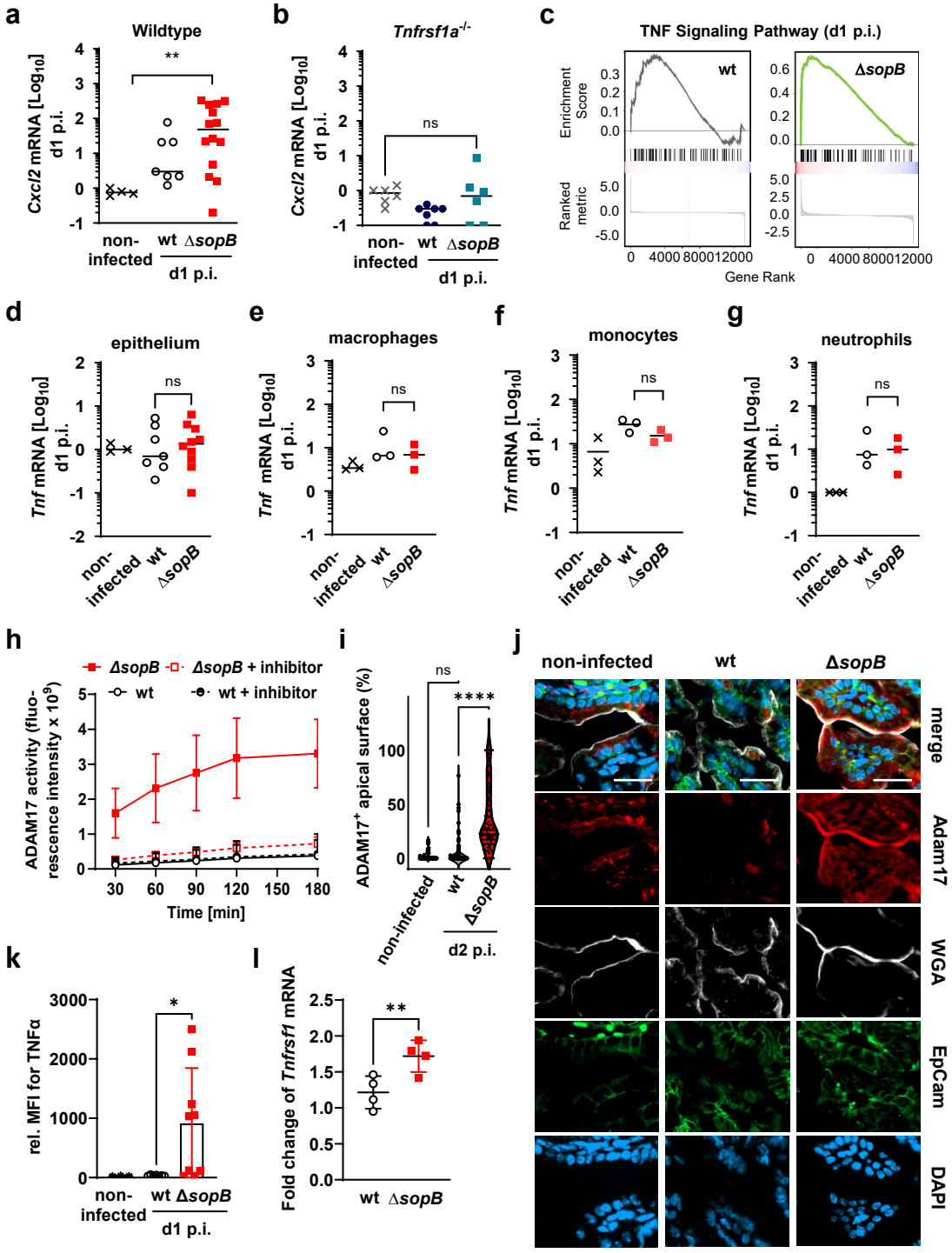

Diab et al., Figure 6

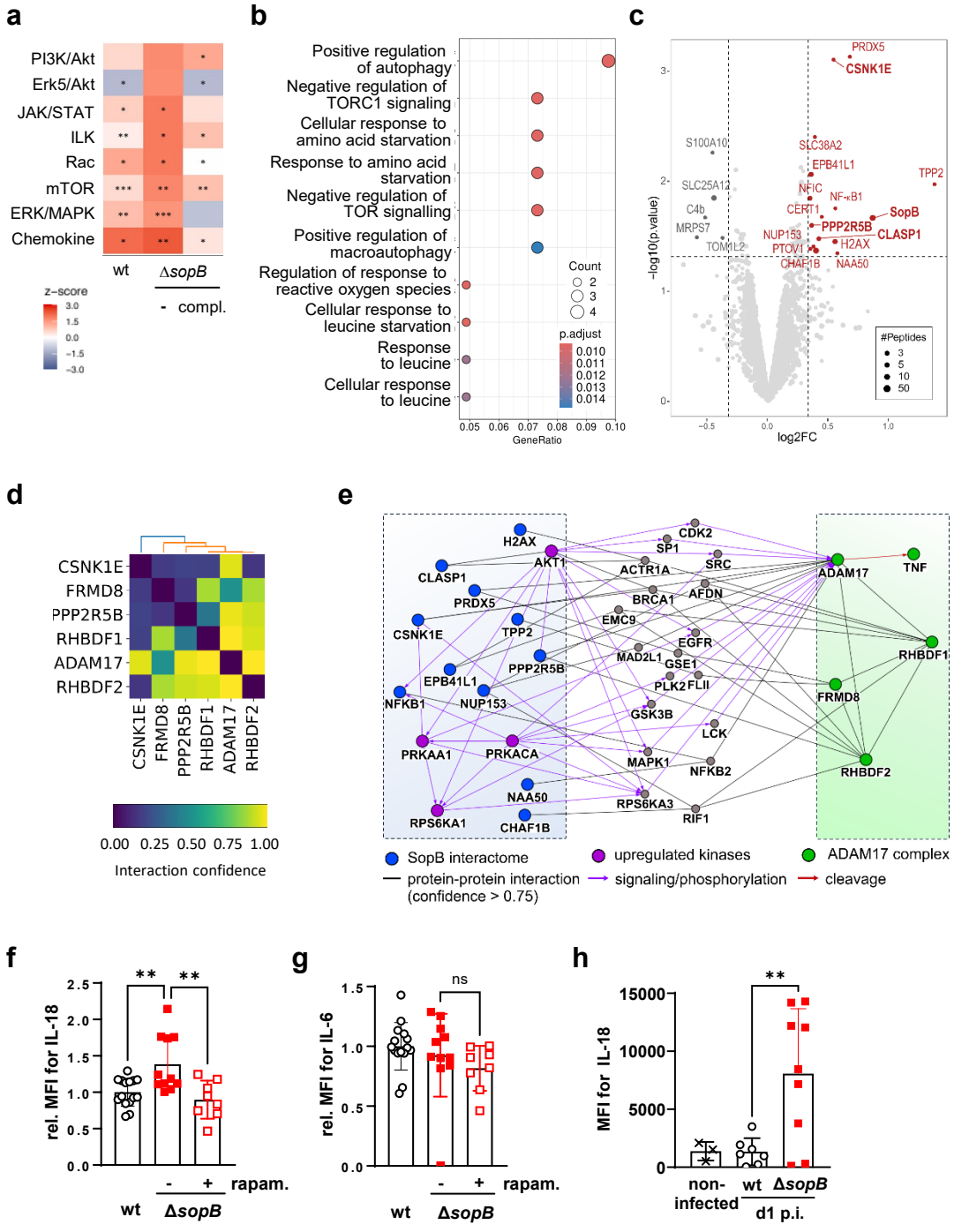

Diab et al., Figure 7